Accepted Manuscript

Tetrahydropyranodiquinolin-8-amines as new, non hepatotoxic, antioxidant, and acetylcholinesterase inhibitors for Alzheimer's disease therapy

Youssef Dgachi, Olga Sokolov, Vincent Luzet, Justyna Godyń, Dawid Panek, Alexandre Bonet, Hélène Martin, Isabel Iriepa, Ignacio Moraleda, Cristina García-Iriepa, Jana Janockova, Lysiane Richert, Ondrej Soukup, Barbara Malawska, Fakher Chabchoub, José Marco-Contelles, Lhassane ismaili

PII: S0223-5234(16)30988-6

DOI: 10.1016/j.ejmech.2016.11.050

Reference: EJMECH 9083

To appear in: *European Journal of Medicinal Chemistry*

Received Date: 13 July 2016

Revised Date: 21 November 2016

Accepted Date: 22 November 2016

Please cite this article as: Y. Dgachi, O. Sokolov, V. Luzet, J. Godyń, D. Panek, A. Bonet, H. Martin, I. Iriepa, I. Moraleda, C. García-Iriepa, J. Janockova, L. Richert, O. Soukup, B. Malawska, F. Chabchoub, J. Marco-Contelles, L. ismaili, Tetrahydropyranodiquinolin-8-amines as new, non hepatotoxic, antioxidant, and acetylcholinesterase inhibitors for Alzheimer's disease therapy, *European Journal of Medicinal Chemistry* (2016), doi: 10.1016/j.ejmech.2016.11.050.

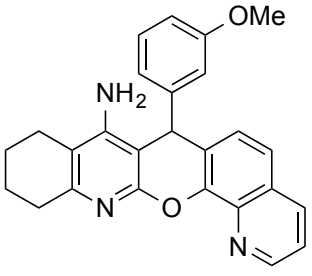

Compound 2h

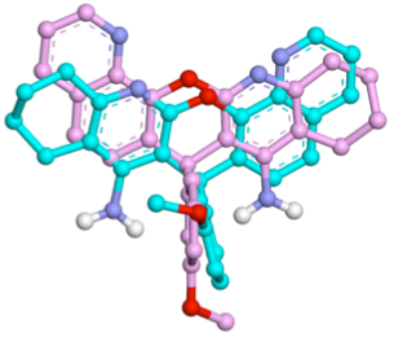

is a permebale, in the low micromolar range
(IC_{50}= 0.75 ± 0.01 μM),
selective, hAChE non-competitive inhibitor,
showing antioxidant, and non-hepatotoxic properties,
fulfilling thus the requirements to be considered a very
promising new tacrine for Alzheimer's disease therapy.

Tetrahydropyranodiquinolin-8-amines as New, non Hepatotoxic, Antioxidant, and Acetylcholinesterase Inhibitors for Alzheimer's Disease Therapy

Youssef Dgachi,[1] Olga Sokolov,[2] Vincent Luzet,[2] Justyna Godyń,[3] Dawid Panek,[3] Alexandre Bonet,[4] Hélène Martin,[4] Isabel Iriepa,[5] Ignacio Moraleda,[5] Cristina García-Iriepa,[6] Jana Janockova,[7] Lysiane Richert,[4] Ondrej Soukup,[7] Barbara Malawska,[3] Fakher Chabchoub,[1]* José Marco-Contelles,[8]* and Lhassane ismaili[2]*

[1]Laboratory of Applied Chemistry: Heterocycles, Lipids and Polymers, Faculty of Sciences of Sfax, University of Sfax. B. P 802. 3000 Sfax-Tunisia
[2] Laboratoire de Chimie Organique et Thérapeutique, Neurosciences intégratives et cliniques EA 481, Univ. Franche-Comté, Univ. Bourgogne Franche-Comté, UFR SMP, 19, rue Ambroise Paré, F-25000 Besançon, France.
[3]Department of Physicochemical Drug Analysis, Jagiellonian University Medical College, Medyczna 9 Street, 30-688 Krakow, Poland.
[4]Laboratory of Cell Toxicology, EA 4267, Univ. Bourgogne Franche-Comté, 19 rue Ambroise Paré, F-25030 Besançon Cedex, France.
[5]Department of Organic Chemistry and Inorganic Chemistry, School of Biology, Enviromental Sciences and Chemistry, University Alcala, Ctra. Barcelona, Km. 33.6, 28871, Alcala de Henares, Spain
[6]Department of Analytical Chemistry, Physical Chemistry, and Chemical Engineering, School of Biology, Enviromental Sciences and Chemistry, University Alcala, Ctra. Barcelona, Km. 33.6, 28871, Alcala de Henares, Spain
[7]Biomedical Research Center, University Hospital Hradec Kralove, Czech Republic
[8]Laboratory of Medicinal Chemistry (IQOG, CSIC) C/ Juan de la Cierva 3, 28006-Madrid, Spain

*****Fakher Chabchoub: fakher.chabchoub@yahoo.fr: Tel.: +216 74676606
*****José Marco-Contelles,: iqoc21@iqog.csic.es; Tel.: + 34915622900
*****Lhassane ismaili: lhassane.ismaili@univ-fcomte.fr Tel.: +33381665543

Abstract

Herein we report an efficient two step synthesis and biological assessment of 12 racemic tetrahydropyranodiquinolin-8-amines derivatives as antioxidant, cholinesterase inhibitors and non-hepatotoxic agents. Based on the results of the primary screening, we identified 7-(3-methoxyphenyl)-9,10,11,12-tetrahydro-7*H*-pyrano[2,3-b:5,6-h']diquinolin-8-amine (**2h**) as a particularly interesting non-hepatotoxic compound that shows moderate antioxidant activity (1.83 equiv Trolox in the ORAC assay), a non competitive inhibition of hAChE (IC_{50}= 0.75 ± 0.01μM), and brain permeable as determined by the PAMPA-Blood Brain Barrier assay.

Keywords: Alzheimer's disease, acetylcholinesterase inhibitors, antioxidants, hepatotoxicity, brain blood barrier, molecular modeling, multifunctional agents

1. Introduction

Alzheimer's disease (AD) is the most common neurodegenerative disorder, affecting round 35 million people worldwide [1]. AD is characterized by progressive memory loss, decline in language skills and other cognitive impairments [2,3]. Although the causes and mechanisms underlying the progress of AD are still not fully understood [4], there is a general consensus about the complexity of the disease. Accordingly, a number of multiple factors, such as the aggregation of beta-amyloid peptide, hyperphosphorylation of tau protein, low levels of acetylcholine (ACh), oxidative stress [5,6] and accumulations of biometals (Cu, Fe, Zn), are playing key roles in the development of AD [7,8].

Nowadays, three acetylcholinesterase inhibitors (AChEIs), donepezil, rivastigmine, and galantamine [9], able to restore ACh levels, and one *N*-methyl-D-aspartate receptor antagonist, memantine [10], are the only available drugs to treat AD patients. These drugs afford modest improvements in memory and cognitive functions, and do not cure or slow the progress of the neurodegeneration [11]. Consequently, there is an urgent need for new drugs for AD therapy.

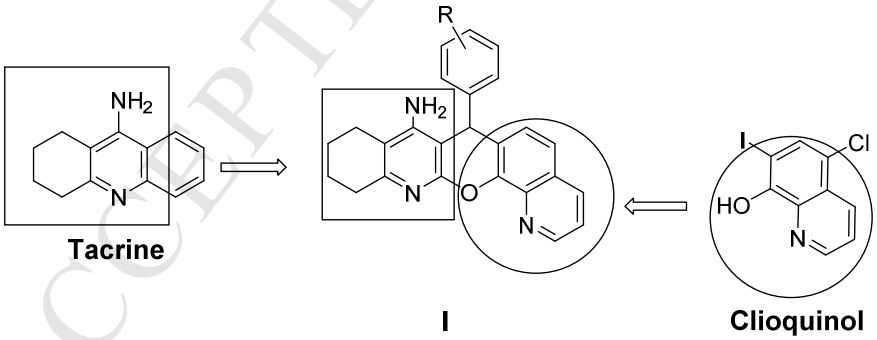

Figure 1 Structures of tacrine, clioquinol, and the new racemic 7-aryl-9,10,11,12-tetrahydro-7*H*-pyrano[2,3-b:5,6-h']diquinolin-8-amine derivatives (**I**) described in this work.

One of the current therapeutic strategies is based on the development of Multi-Target-Directed Ligands (MTDLs), to take into account the multifactorial nature of AD, and consequently, being able to simultaneously interact with the different enzymatic systems or

receptors involved in the pathology [12–17]. In our laboratory, and by using multicomponent reactions (MCR), we have recently prepared a number of new MTDLs as AChEIs showing strong antioxidant power [18–20].

We have now designed new MTDLs based on clioquinol, as an antioxidant, and Cu^{II}-complexing agent [21], and tacrine, one of the most potent known ChEIs to date, although discontinued shortly after its approval due to its hepatotoxicity [22]. Thus, the new tetrahydropyranodiquinolin-8-amine hybrids (**I**) (Figure 1) result from the juxtaposition of both reference molecules and are targeted to act as antioxidant, biometal chelator, and ChEIs. Thus, in this work we have synthesized and evaluated 7-aryl-9,10,11,12-tetrahydro-7*H*-pyrano[2,3-b:5,6-h']diquinolin-8-amine derivatives **2a-l** (Scheme 1), and identified 7-(3-methoxyphenyl)-9,10,11,12-tetrahydro-7*H*-pyrano[2,3-b:5,6-h']diquinolin-8-amine (**2h**) as a new, non-hepatotoxic, antioxidant, AChEI able to cross the brain-blood-barrier (BBB) for the potential AD therapy.

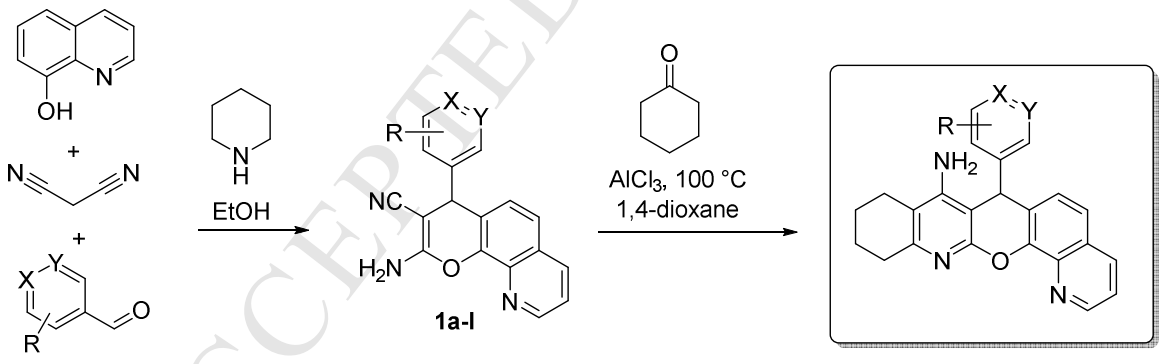

X, Y= C, R= H
X, Y= C, R= 2-F
X, Y= C, R= 3-F
X, Y= C, R= 2-Br
X, Y= C, R= 4-NO_2
X, Y= C, R= 2,6-di-Cl
X, Y= C, R= 2-OCH_3
X, Y= C, R= 3-OCH_3
X, Y= C, R= 4-OCH_3
X, Y= C, R= 4-CH_3
X= N, Y= C R= H
X= C, Y= N, R= 2-Br

2a X, Y= C, R = H
2b X, Y= C, R= 2-F
2c X, Y= C, R= 3-F
2d X, Y= C, R= 2-Br
2e X, Y= C, R= 4-NO_2
2f X, Y= C, R= 2,6-di-Cl
2g X, Y= C, R= 2-OCH_3
2h X, Y= C, R= 3-OCH_3
2i X, Y= C, R= 4-OCH_3
2j X, Y= C, R= 4-CH_3
2k X= N, Y= C, R= H
2l X= C, Y= N, R= 2-Br

Scheme 1. Synthesis of racemic tetrahydropyranodiquinolin-8-amines **2a-l**.

2. Results and discussion

2.1. Synthesis

The synthesis of racemic 7-aryl-9,10,11,12-tetrahydro-7*H*-pyrano[2,3-*b*:5,6-*h'*]diquinolin-8-amines **2a-l** has been carried out in two steps as shown in scheme 1. The first step, a MCR between malononitrile, selected substituted benzaldehydes or pyridincarbaldehydes, and 8-hydroxyquinoline, in the presence of catalytic amounts of piperidine, in ethanol, at 100 °C, for 15 min, gave the known 4*H*-pyrans **1a-l** in very good yield [23], whose Friedlander-type reaction [24] with cyclohexanone, under the usual experimental conditions, afforded the expected racemic compounds **2a-l** (Scheme 1)**.** All new compounds gave analytical and spectroscopic data in good agreement with their structures (**Experimental Part**).

Table 1. Inhibition of *Ee*AChE, hACHE, eqBuChE, (IC_{50}, μM) and ORAC-FL values for compounds **2a-l** , tacrine, clioquinol and ferulic acid.

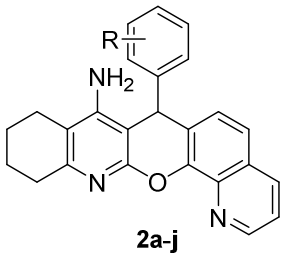

2a-j

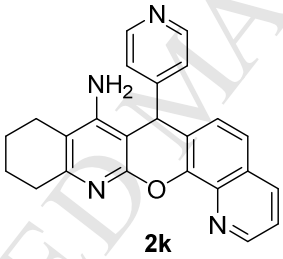

2k

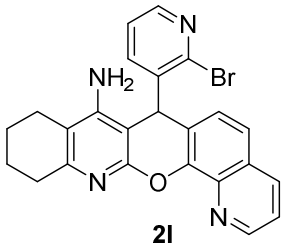

2l

Compound	R	*Ee*AChE[a]	hAChE	eqBuChE[a]	BBB	ORAC
2a	H	0.06±0.01	1.73 ± 0.02	1.11±0.00	-[c]	1.47±0.25
2b	2-F	0.11±0.01	-[c]	0.63±0.08	-[c]	1.49±0.09
2c	3-F	0.09±0.01	2.20 ± 0.03	-[d]	-[c]	1.36±0.05
2d	2-Br	0.14±0.01	-[c]	0.21±0.02	-[c]	2.01±0.05
2e	4-NO_2	0.24±0.01	-[c]	-[d]	-[c]	2.49±0.19
2f	2,6-di-Cl	0.10±0.01	-[c]	-[d]	-[c]	1.22±0.07
2g	2-OCH_3	0.08±0.01		1.51±0.10	-	1.60±0.22
2h	**3-OCH_3**	**0.04±0.01**	**0.75 ± 0.01**	**1.30±0.22**	**5.41 ± 0,3[b]**	**1.83±0.10**
2i	4-OCH_3	0.04±0.01	1.51 ± 0.02	1.30±0.19	-[c]	1.71±0.10
2j	4-CH_3	0.04±0.01	2.85 ± 0.05	0.53±0.03	-[c]	1.88±0.35
2k	-	0.47±0.07	-[d]	-[d]	-[c]	1.70±0.12
2l	-	0.19±0.00	-[d]	2.86±0.18	-[c]	2.35±0.26
Tacrine	-	0.03±0.01	0.13±0.00	0.05±0.01nM	-[c]	0.2±0.1
Ferulic acid	-	-[c]	-[c]	-[c]	-[c]	3.74±0.22

[a] Inhibition curves were obtained by nonlinear regression. *Ee*: electric eel, eq: equine. Each IC_{50} value is the mean ± SEM of quadruplicate of at least three different experiments. Results are expressed in μM; [b] PAMPA method (Pe ± SEM (*10^{-6} cm s^{-1}); [c]Not determined ; [d] No inhibition.

2.2. Biological evaluation

2.2.1. Evaluation of AChE and BuChE inhibition

The preliminary evaluation of the inhibitory potencies against *Electrophorus electricus* AChE (*Ee*AChE) and serum horse BuChE (eqBuChE) was carried out following the Ellman's protocol [25], using tacrine as reference compound for comparative purposes. As shown in table 1, these compounds exhibited low micromolar inhibitory potencies against *Ee*AChE with IC_{50} values ranging from 0.04 and 0.47 μM, for compounds **2h** and **2j**, respectively. Notably, compounds **2a**,**c**,**g-i** showed IC_{50} not exceed 100 nM. Among them, compound **2c** (IC_{50}= 0.09 μM) was 3-fold less active than tacrine (IC_{50}= 0.03 μM), but totally selective against eqBuChE. The most potent *Ee*AChEIs were **2h-j**, all with the same IC_{50} value equal to 0.04 μM, in the same range of tacrine (IC_{50}= 0.03 μM). Regarding the eqBuChE inhibition eight products (**2a**, **2b**, **2d**, **2g-j**, and **2l**) showed micromolar inhibition ranging between 0.21 and 2.86 μM, the most potent being **2d** (IC_{50}= 0.21 μM), whereas compounds **2c**, **2e**, **2f** and **2k** showed no inhibition at all.

Regarding the structure-activity relationship, and for the inhibition of AChE, several conclusions can be drawn. First of all, compounds bearing substituted aryl rings attached to C7 at the pyran core (**2a-d**, **2f-j**) are more potent AChEIs than those bearing a pyridine ring (**2k**,**l**), except for compound **2e**, substituted with a nitro group at C4'. Among the substituted aryl derivatives, it is clear that the unsubstituted (**2a**) or those bearing electron-donor substituents (**2g-j**) are more potent AChEIs than those bearing electron-withdrawing rings (**2b-f**). To sum up, and regarding the positions of substituents at the aromatic ring at C7, compounds **2b-f** bearing a substituent at position C3', and those (**2g-j**) bearing it at positions C3' or C4', gave the best inhibition. It is also apparent that among compounds **2g-j**, the type of the substituent (Me *vs* OMe) or the position of the methoxy group in the aromatic ring has no effect on the AChE inhibition power, showing similar IC_{50} values. For the inhibition of

BuChE, no evident SAR could have been established. The tested compounds exhibited a lower inhibitory potency against eqBuChE compared to *Ee*AChE or complete lack of activity. Therefore, only the most potent inhibitors **2a**,**c**,**h-j** against *Ee*AChE were tested for their ability to inhibit human AChE (hAChE). As shown in table 1, these five compounds had an activity ranking from 2.85 μM for **2j** to 0.75 μM for **2h**, being again the most potent hAChE inhibitor, only 5.7 fold less active than tacrine. In summary, the best inhibitor was compound **2h**, bearing methoxygroup at position C3' of aryl ring attached to C7 at the pyran core, as strongly inhibited *Ee*AChE, hAChE and eqBuChE in the low micromolar range, showing IC_{50} values equal to 0.04 ± 0.01 μM, 0.75 ± 0.01 μM, and 1.30 ± 0.22 μM, respectively.

*2.2.2. Kinetic study of the hAChE inhibition by compound **2h***

The kinetic mechanism of hAChE inhibition of compound **2h** has been investigated by obtaining the Lineweaver-Burk double reciprocal plots (Figure 2), whose analysis showed that K_m appeared unaltered while V_{max} decreased at increasing concentrations of the inhibitor. This pattern indicates that inhibitor **2h** acts as a non-competitive enzyme inhibitor. Replots of the slope versus concentration of compound **2h** give an estimate of the inhibition constant, which is equal to 0.87 μM.

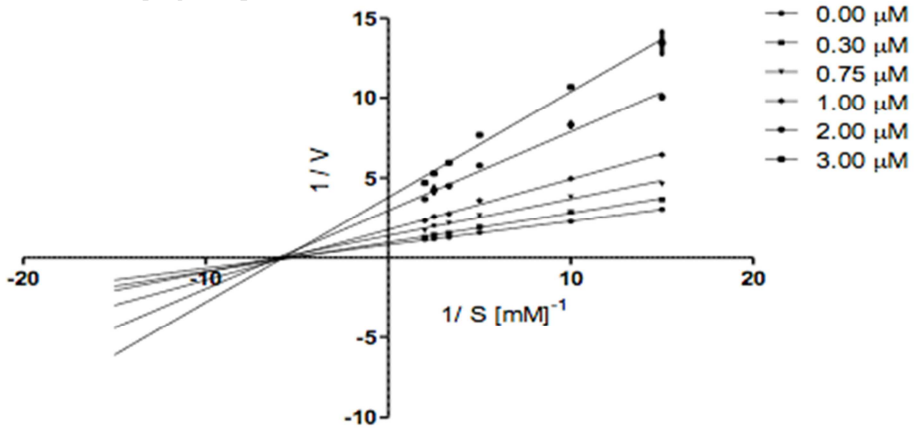

Figure 2. Lineweaver – Burk plot illustrating non-competitive type of hAChE inhibition by compound **2h**. S = acetylthiocholine; *V* = initial velocity rate.

2.2.3. ORAC test

Next, we assessed the antioxidant activity of racemic compounds **2a-l** using the Oxygen Radical Absorbance Capacity (ORAC-FL) method [26,27]. Tacrine and ferulic acid [28] were used as negative and positive reference molecules, respectively. Results are expressed in relation to radical scavenging properties of Trolox yielding the Trolox equivalents (TE) unit. As shown in table 1, all compounds presented good radical scavenging properties with ORAC values ranging from 1.22 to 2.49 TE, but lower than the value found for ferulic acid (3.7 TE). The three most potent antioxidants were compounds **2d** (2.01 TE)**, 2l** (2.35 TE) and **2e** (2.49 TE)**,** bearing a 2'-bromophenyl, 2'-bromopyridyl, and a 4'-nitrophenyl group attached to pyran ring at C7, respectively. This trend clearly means that stronger the electron-withdrawing effect of the aromatic ring at C7 is, higher the antioxidant capacity observed. Thus, for compounds of type **2**, we hypothesize that the presence of a free (C8)-NH_2 could explain the observed antioxidant effect, due the lability of the N-H bond against any radical oxygenated species.

2.2.4. Studies of metal-chelating properties

The ability of compound **2h** to chelate biometals such as Cu^{2+}, and Fe^{2+} was next studied by UV–vis spectrometry. As shown, the maximum absorption wavelength remained unchanged when $CuSO_4$ was added and incubated for 60 min and 20 h (**Supplementary Material**). The same trend was observed for $FeSO_4$ (**Supplementary Material**), suggesting that unfortunately little or no complex formation between compound **2h** with these cations took place. In order to explain these unexpected results, a Density Functional Theory (DFT) study was conducted to investigate the complexation between the ligand and the Cu(II) metal ion, and understand the intrinsic factors affecting cation complexation.

Thus, the pyranopyridoquinoline (PPQ) system was used as a simplified model of compound **2h**. As shown in figure 3, two distinct complexes of Cu^{2+} with PPQ have been considered. In the $Cu(PPQ)SO_4$, the metal cation is bonded to one ligand, PPQ, in a bidentate chelating mode and to two oxygens atoms of the sulphate anion resulting in a square-planar environment. On the other hand, modelled $Cu(PPQ)SO_4(MeOH)$ adduct consists of five coordinated copper (II) complex with the oxygen and the nitrogen of PPQ bonded to the metal ion and the two oxygen atoms of the sulphate anion. One further oxygen atom of one methanol molecule is finally coordinated to the copper ion resulting in a square based pyramidal environment.

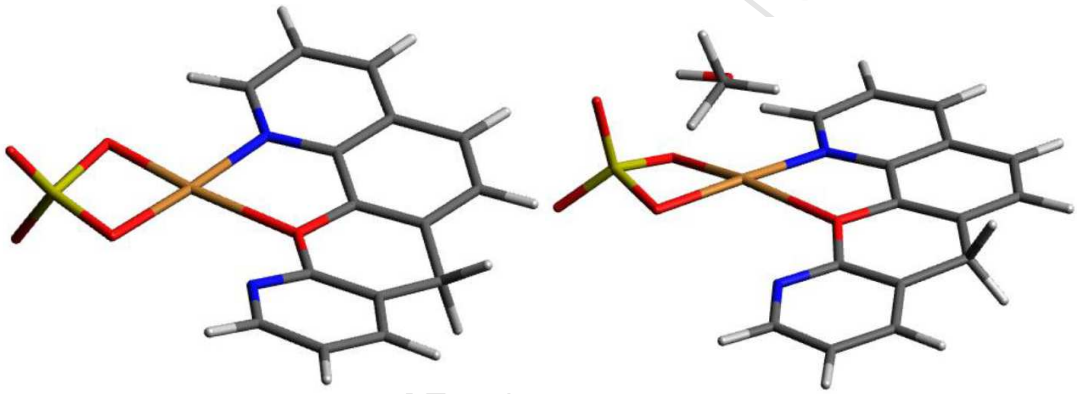

$Cu(PPQ)SO_4$ $Cu(PPQ)SO_4(MeOH)$

Figure 3. B3LYP-optimized structures for Cu^{2+} complexes of PPQ.

The total energy of each complex was calculated and compared with that of the sulphate complex [Cu (II) $(MeOH)_x(SO_4)$] as a reference to quantitatively evaluate the stability of each complex. Table 2 shows the formation energy of each complex, calculated using equations I and II.

Table 2. Thermodynamic functions of the copper (II) complexes with PPQ.

Complex	ΔH(Kcal/mol)	ΔG(Kcal/mol)
$Cu(PPQ)(SO_4)$	0.61	-7.85
$Cu(PPQ)(SO_4)(MeOH)$	5.69	-2.77

$$[E\,(Cu(PPQ)(SO_4) + 2\,E(MeOH)] - [E(PPQ) + E\,(Cu\,(II)\,(MeOH)_2(SO_4)] \quad (I)$$

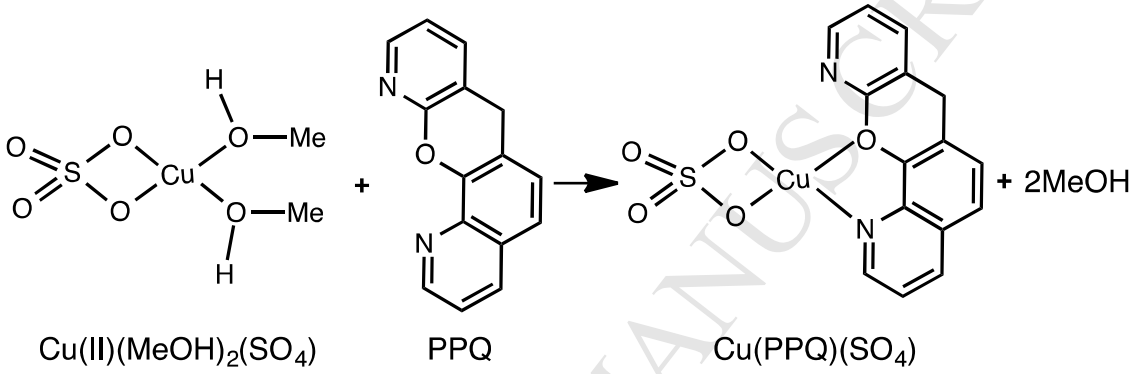

$$[E\,(Cu(PPQ)(SO_4)(MeOH)\,) + 2\,E(MeOH)] - [E(PPQ) + E\,(Cu\,(II)\,(MeOH)_3(SO_4)] \quad (II)$$

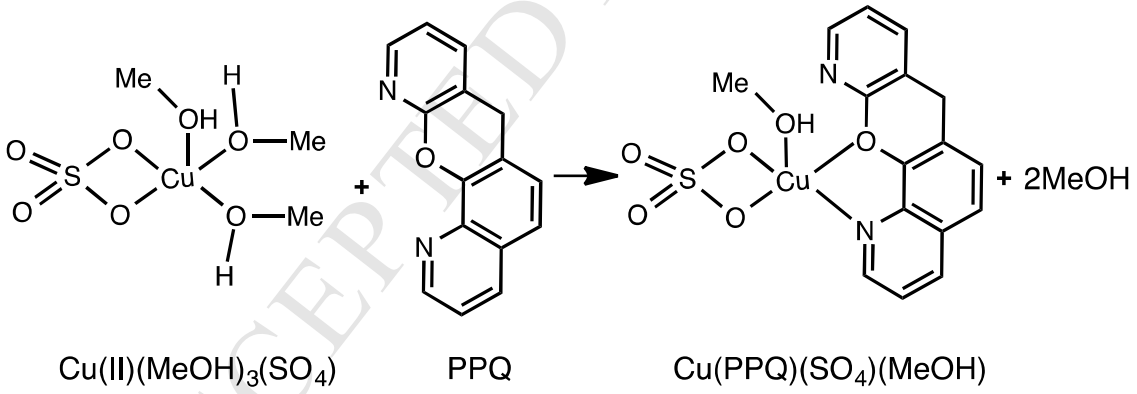

Scheme 2. Chemical equations used to measure the formation energies of the complexes $[Cu(II)(PPQ)(MeOH)_x(SO_4)]$.

The most important point gathered from table 2 is that the PPQ system does not have the capability to form stable metal complexes with Cu^{2+} since it has positive formation energy of 0.61 and 5.69 Kcal/mol. Interestingly, a comparison between formation energies values of $Cu(PPQ)(SO_4)$ and $Cu(PPQ)(SO_4)(MeOH)$ complexes shows that these values depend on the

number of molecules coordinated to the metal. Therefore, the formation of the complex with four ligands is clearly favored with respect to the complex with five ligands, suggesting that an increase of the steric hindrance around the metal decrease the stability of the corresponding complex.

Both complexations are endothermic, however the Gibbs free energy of the complex formation was calculated as -7.85 and -2.77 Kcal/mol, which are negative values. The positive formation energy of the two complexes could be explained by the destabilizing effect of the pyridine ring fused to the pyran ring. On one hand, the electron-withdrawing ability of this ring makes the oxygen-pyran a worse electron donor, decreasing the interaction strength between the cooper and the oxygen atoms. On the other hand, its nitrogen atom is far enough from the cooper atom to coordinate but close enough to probably generate an electrostatic repulsion between the lone pair of this nitrogen atom and the electronic density (*e.g.* electrons located in d orbitals) of the cooper atom.

To explore the effect of pyridine ring on the complex formation, a phenyl ring has substituted it leading to the ligand PhePQ (Figure 4). In scheme 3 we show the equations used to compute the formation energies of the complexes starting from this ligand.

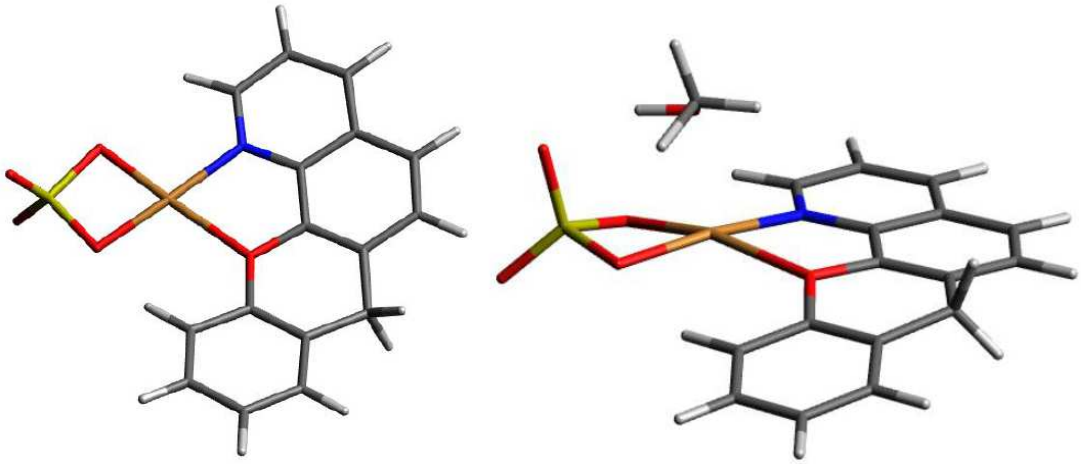

Cu(PhePQ)(SO_4) Cu(PhePQ)(SO_4)(MeOH)

Figure 4. B3LYP-optimized structures for Cu^{2+} complexes of PhePQ.

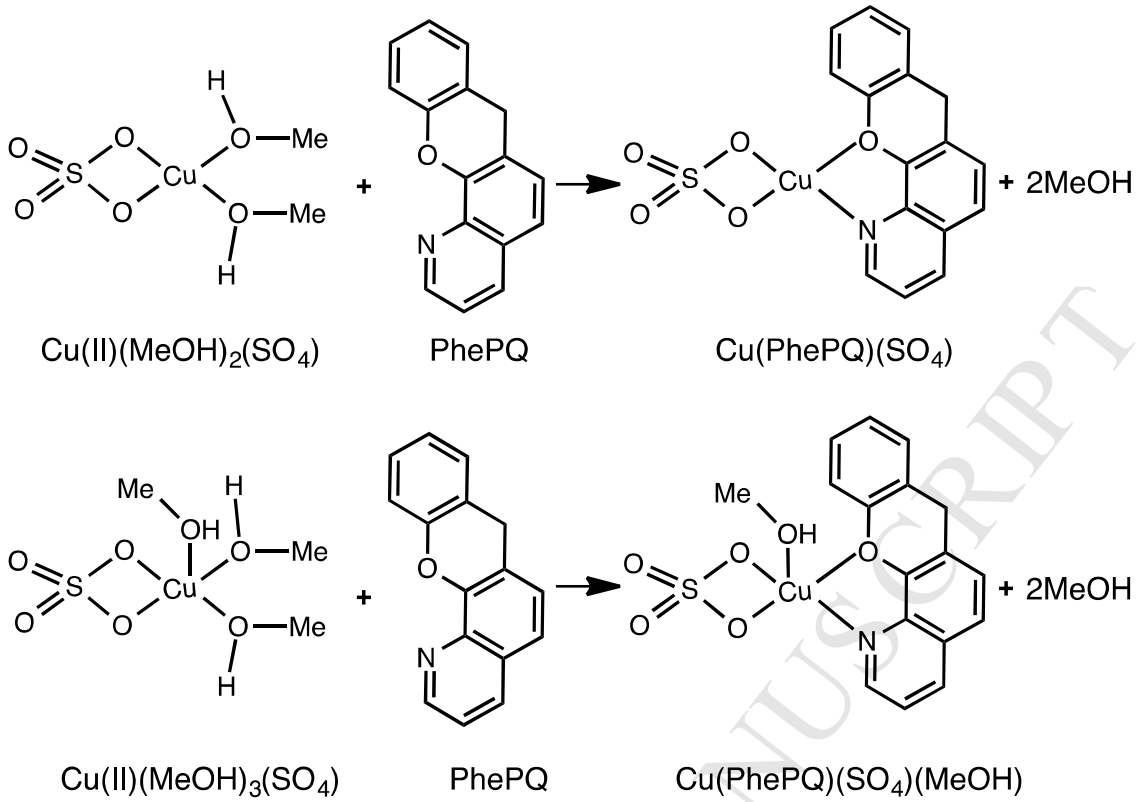

Scheme 3. Chemical equations used to measure the formation energies of the complexes [Cu(PhePQ)$(MeOH)_x(SO_4)$].

ΔH and ΔG of [Cu(II)(PhePQ)$(MeOH)_x(SO_4)$] complexes (Table 3) were computed and compared with the corresponding values for [Cu(II)(PPQ)$(MeOH)_x(SO_4)$] complexes (Table 3).

Table 3. Thermodynamics functions of the copper (II) complexes with PhePQ.

Complex	ΔH(Kcal/mol)	ΔG(Kcal/mol)
Cu(PhePQ)(SO_4)	-2.02	-9.99
Cu(PhePQ)(SO_4)(MeOH)	3.52	-4.22

The energy of formation for the less crowded system, Cu(PhePQ)(SO_4), is more favorable than for Cu(PhePQ)(SO_4)(MeOH) by ~5 Kcal/mol with respect to both ΔH and ΔG. Moreover, comparing the energies of formation of complexes Cu(PPQ)(SO_4) and

Cu(PhePQ)(SO_4) it is observed that ΔH becomes negative for the later, indicating that in this case the formation of Cu(PhePQ)(SO_4) is energetically favorable, suggesting a clear effect of the pyridine ring.

To explore the effect of the pyridine ring on the geometrical parameters of chelated ring and the metal-oxygen structure, the geometrical parameters of Cu(PhePQ)(SO_4) were compared with the corresponding values for Cu(PPQ)(SO_4). The O-cα-pyrane ring bond length in Cu(PhePQ)(SO_4) slightly increases while the Cu-O and Cu-N bond lengths slightly decrease compared to the corresponding values in Cu(PPQ)(SO_4).

These results indicate the formation of more stable complex between Cu(II) and PhePQ compared with that between Cu(II) and PPQ (see Table 4).

Table 4. Selected theoretical geometrical parameters for Cu(PPQ)(SO_4) and Cu(PhePQ)(SO_4) complexes[a].

Complex	d_{C-O}	d_{Cu-O}	d_{Cu-N}
Cu(PPQ)(SO_4)	1.397	2.321	1.994
Cu(PhePQ)(SO_4)	1.410	2.260	1.971

[a] d, bond distance in Å.

In addition, comparison between the atomic charges in the Cu(PPQ)(SO_4) and Cu(PhePQ)(SO_4) complexes show that the O atom in Cu(PhePQ)(SO_4) is more negative than that in Cu(PPQ)(SO_4) (Table 5). This difference has been attributed to the resonance conjugation between the electron-withdrawing pyridine ring and the chelated ring of PPQ. This resonance conjugation, which causes less electron delocalization in the chelated ring of Cu(PPQ)(SO_4) compared to that of Cu(PhePQ)(SO_4), is responsible for the shorter O-cα-pyrane ring bond in the former (Table 5).

Charge transfer from the pyrane to the pyridine acceptor, will decrease the oxygen-electron density that is available to transfer to the metal, therefore the electron-withdrawing ability of substituents influences ligand affinity.

Table 5. Selected atomic charges for $Cu(PPQ)(SO_4)$ and $Cu(PhePQ)(SO_4)$ complexes.

Complex	O charge
$Cu(PPQ)(SO_4)$	-0.476
$Cu(PhePQ)(SO_4)$	-0.517

*2.2.5. In vitro cytotoxicity of compounds **2a**, **2c** and **2h-j** in HepG2 cells*

For an effective lead drug, the cytotoxicity should be at the lowest possible level. In this sense, we submitted the five most promising compounds **2a**, **2c** and **2h-j** to an *in vitro* toxicologic evaluation (MTT assay) using human hepatocellular carcinoma cell line (HepG2) [29] which represents a well accepted probe to evaluate hepatotoxic effect, using different dose concentrations (1, 10, 30, 100, 300, 1000 μM). As shown in table 6, where, tacrine showed no decrease in cell viability up to 100 μM, but exerts a marked cytotoxicity above 300 μM. The five tested compounds, except

Table 6. *In vitro* cytotoxicity of tacrine, **2a**, **2c** and **2h-j** in HepG2 cells.

	30 μM	**100 μM**	**300 μM**	**1000 μM**
Tacrine	106.4 ± 6.1	110.5 ± 5.8	49.3 ± 3.7***	13.7 ± 3.1***
2a	108.6 ± 12.8	102.2 ± 11.2	93.7 ± 11.5	91.2 ± 6.4
2c	92.4 ± 3.4	95.4 ± 11.5	91.6 ± 13.9	75.8 ± 5.7*
2h	110.0 ± 3.5	102.2 ± 5.2	94.0 ± 7.4	94.1 ± 3.0
2i	115.4 ± 1.7	110.7 ± 3.8	113.8 ± 4.0	104.7 ± 1.4
2j	115.9 ± 4.9	106.0 ± 1.5	92.5 ± 5.9	96.2 ± 4.8

Means ± SEM of triplicates from at least three different cultures. *p<0.05, ***p<0.001, as compared to the control cultures (one-way ANOVA).

2c, had no significant cytotoxic effects measured in concentrations up to 1000 μM on HepG2 cells and could be considered as non-hepatotoxic. Although compound **2c** displayed a hepatotoxic effect at 1000 μM it is still much less cytotoxic than tacrine.

2.2.6 *In vitro cytotoxicity of compounds **2h** in primary human hepatocytes*

Primary human hepatocytes are considered the gold standard for the evaluation and prediction of hepatotoxicity in humans [30], therefore we evaluated the most active compound **2h** on human hepatocytes. Pools of cryopreserved primary human hepatocytes used in suspension have been described as useful for the screening of hepatotoxicants [31,32]. Thus a suspension of human hepatocytes cells from a pool of 9 donors was used with seven concentrations (0.1, 0.3, 1.0, 3.0, 10.0, 30. 0 and 100.0 μM) with respect of the solubility limits of compounds in treatement medium. As shown in Table 7, tacrine, displayed cytotoxicity towards the pool of primary human hepatocytes from 30.0 μM while compound 2h did not exhibit any cytotoxicity until 100.0 μM.

Table 7. *In vitro* concentration-response of tacrine and **2h** on primary human *hepatocyte viability*

Concentration	00 μM	0.1 μM	1.0 μM	3.0 μM	10.0 μM	30.0 μM	100.0 μM
Tacrine	100 ± 11	94 ± 3	86 ± 3	83 ± 5	81 ± 7	75 ± 14	70 ± 3
2h	100 ± 11	89 ± 4	84 ± 8	83 ± 8	89 ± 3	99 ± 11	89 ± 2

Results expressed in Means ± SD of triplicates from from a pool of 9 donors

2.2.7. PAMPA assay

Prediction of blood-brain barrier penetration for the most potent hAChEI **2h** shows high probability to cross the BBB *via* passive diffusion (Table 1). The data obtained have been correlated to standard drugs, where CNS availability is known and also reported using the

PAMPA assay [33], showing high resemblance with previously reported penetrations as well as with a general knowledge about the availability in the CNS of such standard drugs.

3. Molecular modeling of compound 2h

To help us understand the observed experimental activities, molecular docking studies were carried out using AutoDock Vina software[34] to obtain the plausible binding mode of the compounds**,** within the active site gorge of hAChE**.** The kinetic data provide evidence that compound **2h** displays a non-competitive inhibition and argue in favour of interactions of **2h** with the PAS of hAChE. Molecular modeling studies have been carried on the most potent hAChE, compound **2h**, in order to validate this assumption.

The C7 carbon of the pyran ring is chiral and two isomers are possible. As the inhibitors were tested as racemic mixtures in the assay, both enantiomeric forms were built up and used for docking to check the effect of chirality on potency and selectivity towards hAChE. The most favorable docking pose for (*R*)-**2h** in the binding site of hAChE is illustrated in figure 5.

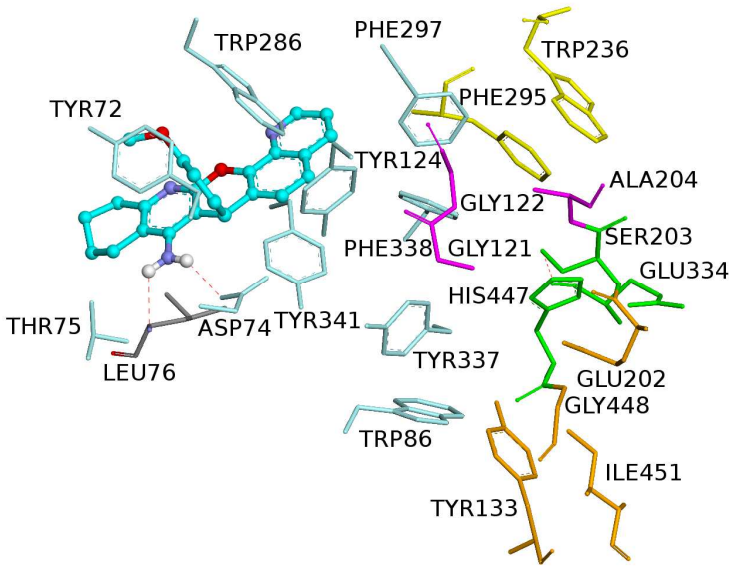

Figure 5. Binding mode of (*R*)-**2h** at the active site of hAChE: Binding affinity = -11.3 Kcal mol^{-1}. The compound is rendered as balls and sticks and illustrated in blue. The side chains conformations of the mobile residues are illustrated in the same light color that the ligand. Different sub-sites of the active site were coloured: catalytic triad (CT) in green, oxyanion hole (OH) in pink, anionic sub-site (AS) in orange, except Trp86, acyl binding pocket (ABP) in yellow, except Phe297 and Phe338, and peripheral anionic sub-site (PAS) in violet**.** Red dashed lines are drawn among atoms involved in hydrogen bond interactions.

The docking results reveal that the *R*-enantiomer is accommodated rather far from the active site, at the top of the gorge (PAS), within the hydrophobic pocket formed by several aromatic residues Tyr72, Tyr124, Trp286, Phe295, Phe297, Tyr337, Phe338 and Tyr341 (Figure 6). The intermolecular interactions are mostly contributed by aromatic-aromatic ring interactions since the ligand contains aromatic rings favoring the ring-ring interactions. The phenyl moiety showed T-shaped interactions with Tyr72 and face to face interaction with Trp286. The quinoline moiety is also interacting with Trp286 and Trp341, through π–π interactions. This enantiomer is bound to the AChE in a manner through its amino group projecting toward the carboxylate group of Asp74 and the amino group of Leu76 forming two hydrogen bonds between the amino group and Asp74 and Leu76 (Figure 6).

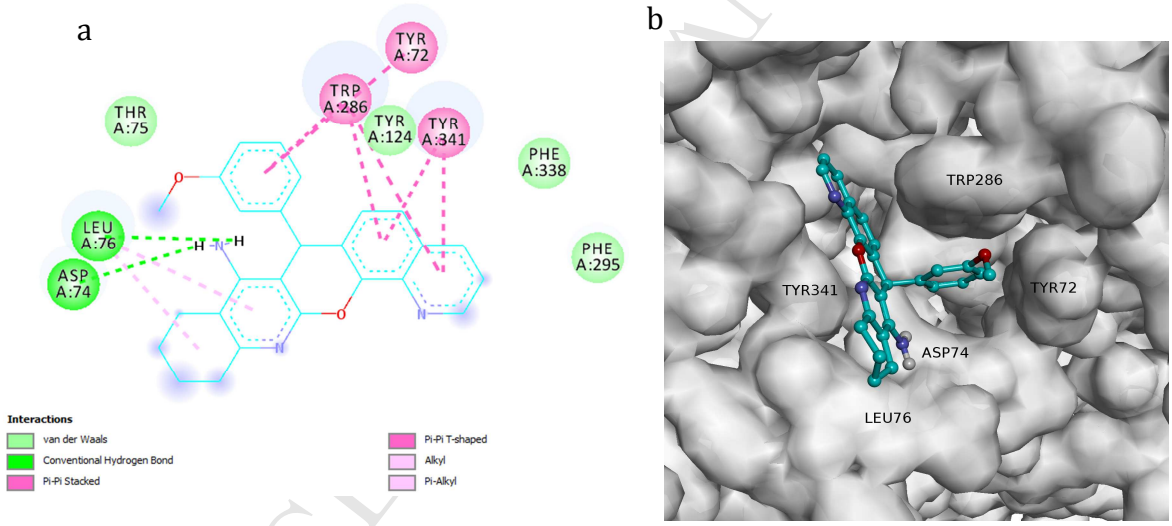

Figure 6. a) Schematic representation of different interactions of (*R*)-**2h** with hAChE. b) Top view of the accessible surface of the active site gorge**.**

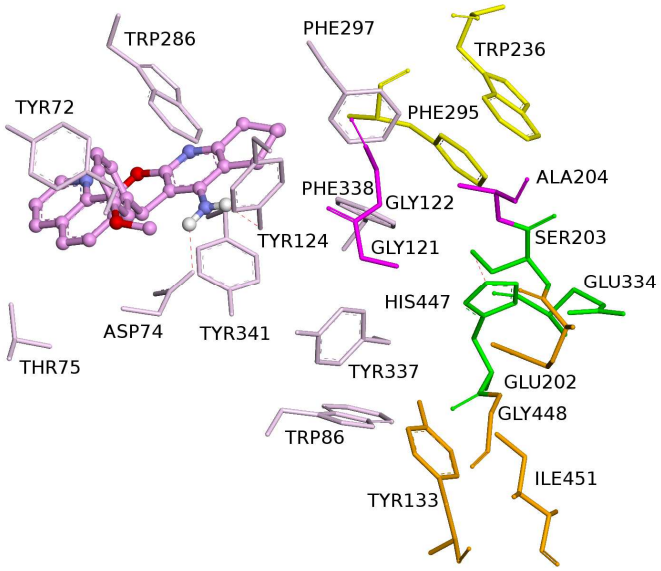

Figure 7. Binding mode of (*S*)-**2h** at the active site of hAChE: Binding affinity = -10.8 Kcal mol^{-1}; The compound is rendered as balls and sticks and illustrated in pink. The side chains conformations of the mobile residues are illustrated in the same light color that the ligand. Different sub-sites of the active site were coloured: catalytic triad (CT) in green, oxyanion hole (OH) in pink, anionic sub-site (AS) in orange, except Trp86, acyl binding pocket (ABP) in yellow, except Phe297 and Phe338, and peripheral anionic sub-site (PAS) in violet**.** Red dashed lines are drawn among atoms involved in hydrogen bond interactions.

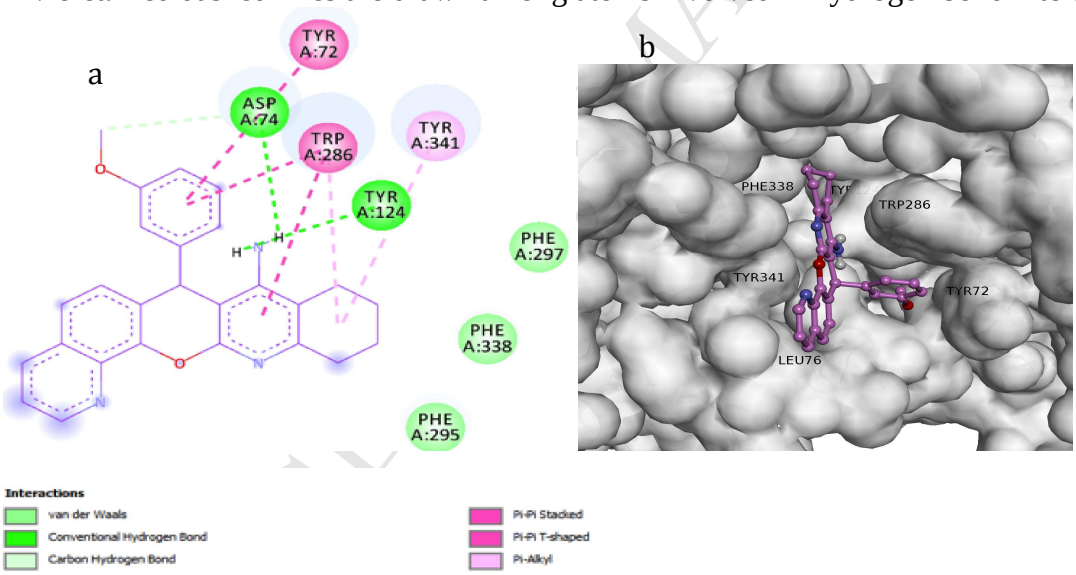

Figure 8. a) Schematic representation of different interactions of (*S*)-**2h** with hAChE.
b) Top view of the accessible surface of the active site gorge.

Docking simulations revealed that the best-scored docking conformation for (*S*)-**2h** showed a binding pattern very similar to that of (*R*)-**2h (**Figure 7). At the top of the gorge, the phenyl moiety showed T-shaped interactions with Tyr72 and face-to-face interactions with Trp286. The pyridine moiety is also interacting with Trp286 through π–π interactions. Cyclohexane

moiety was well fitted in the hydrophobic pocket composed by Phe295, Phe297 and Phe338. The amino group of the ligand forms hydrogen bond with Asp74 carboxylate group and with the hydroxyl group of the Tyr124 (Figure 8).

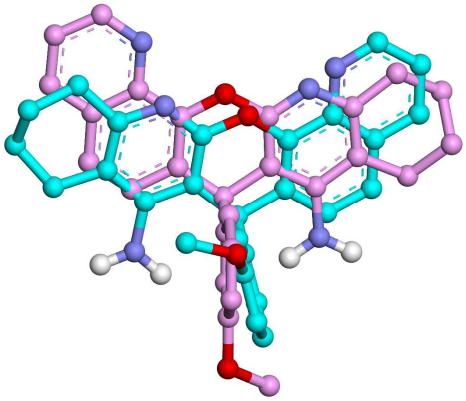

Figure 9. Overlay of binding mode of compound (*R*)-**2h** (blue) and (*S*)-**2h** (pink) in hAChE.

The best docked poses of both enantiomers were superposed and showed to be similarly docked in the gorge of hAChE. The detailed picture of the superimposed docking poses of (*R*)-**2h** and (*S*)-**2h** is shown in figure 9. They share the position of the central cores of the ligands (methoxyphenol-pyran moieties) and this implies that quinoline moiety of each enantiomer occupies a similar position as the tetrahydroquinoline moiety of the other. This binding pattern to the hAChE has already been observed on 7-aryl-9,10,11,12-tetrahydro-7H-benzo[7,8]chromeno[2,3-b]quinolin-8-amines [35].

4. Conclusions

To sum up, we synthesized and evaluated twelve new racemic tetrahydropyranodiquinolin-8-amines derivatives as promising multifunctional compounds for the potential AD therapy. As a result, we have identified racemic 7-(3-methoxyphenyl)-9,10,11,12-tetrahydro-7*H*-pyrano[2,3-b:5,6-h']diquinolin-8-amine (**2h**) as suitable compound for further development, as this compound is non hepatotoxic, shows moderate antioxidant activity (1.83 equiv Trolox), crosses the BBB in the PAMPA assay, is a good hAChEI (IC_{50}= 0.75 ± 0.01 μM) in

the low micromolar range, showing non-competitive inhibition mechanism, binding presumably at the peripheral binding site of AChE, an hypothesis that has been confirmed by carrying out molecular modeling of both enantiomers.

5. Materials and Methods

5.1. Chemistry methods

Melting points were determined on a Kofler apparatus (Wagner Munz), and are uncorrected. The reactions were monitored with TLC using aluminium sheets with silica gel 60 F254 from Merck. IR spectra were performed on a Perkin-Elmer PARAGON FT-IR spectrometer. NMR ^{1}H and ^{13}C were recorded on a Bruker spectrometer using $CDCl_3$ or DMSO.d_6 as solvents. The chemical shifts are reported in parts per million (ppm), using tetramethylsilane (TMS) as internal reference. The multiplicities of the signals are indicated as follow: br, broad; s, singlet; d, doublet; t, triplet; q, quadruplet; and m, multiplet, the coupling constants are expressed in Hz. Elemental analysis were performed on Thermofinnigan Flash EA 1112. The microwave assisted reactions were carried out in synthetic microwave (microwave Anton Paar 300) with a maximum power of 300 W.

*5.1.1. General procedure for the of compounds **1a-l**.*

A mixture of aromatic aldehyde (0.01 mmol), malononitrile (0.01 mmol), and 8-hydroxyquinoline (0.01 mmol) in ethanol (15 ml) in the presence of piperidine (0.5 equiv) was warmed at 100 °C until complete precipitation. (reaction times: 15 min). The solid obtained was collected by filtration and recrystallised from ethanol, and dried, to give compounds **1a-l** in good yield.

*5.1.1.1. 2-Amino-4-phenyl-4H-pyrano[3,2-h]quinoline-3-carbonitrile (**1a**).* Yield: 92 %; mp 196-198 °C; IR (KBr) ν_{max} 2225 (CN), 3526, 3445 (NH_2) cm^{-1}; ^{1}H NMR (300 MHz, DMSO-d_6) δ 8.94-7.22 (m, 10Harom), 7.12 (br s, 2H, NH_2), 4.95 (s, H_{pyran}); ^{13}C NMR (75 MHz,

DMSO-d_6) δ 160.6 (C), 150.6 (C), 146.1 (CH), 143.3 (C), 137.8 (C), 136.4 (CH),133.5 (CH), 129.1 (CH), 128.1 (CH), 127.4 (C), 127.3 (C), 126.9 (CH), 123.9 (CH), 122.5 (CH), 122.3 (CH), 121.4 (CH), 120.8 (CN), 56.2 (C), 41.1 (CH).

*5.1.1.2. 2-Amino-4-(2-fluorophenyl)-4H-pyrano[3,2-h]quinoline-3-carbonitrile (**1b**).* Yield: 93%; mp 251-2 °C; IR (KBr) ν_{max} 2190 (CN), 3409, 3310 (NH_2) cm^{-1}; ^1H NMR (300 MHz, DMSO-d_6) δ 8.90-7.12 (m, 9Harom), 5.06 (br s, 2H, NH_2), 4.93 (s, H_{pyran}); ^{13}C NMR (75 MHz, DMSO-d_6) δ 161.9 (C), 157.2 (C), 151.6 (C), 144.1 (C), 137.9 (C), 136.8 (CH), 135.2 (CH), 129.1 (CH), 128.2 (C), 127.8 (C), 126.1 (CH), 123.8 (CH), 122.1 (CH), 121.7 (CH), 121.0 (CH), 120.3 (CH), 120.1 (CN), 58.2 (C), 41.6 (CH).

*5.1.1.3. 2-Amino-4-(3-fluorophenyl)-4H-pyrano[3,2-h]quinoline-3-carbonitrile (**1c**).* Yield: 84%; mp 249-250 °C; IR (KBr) ν_{max} in cm^{-1}: 2190 (CN), 3409, 3310 (NH_2). ^1H NMR (300 MHz, DMSO-d_6) δ 8.96-7.14 (m, 9Harom), 5.06 (br s, 2H, NH_2), 4.92 (s, H_{pyran}); ^{13}C NMR (75 MHz, DMSO-d_6) δ 160.9 (C), 157.9 (C), 151.8 (C), 143.7 (C), 137.6 (C), 136.2 (CH), 135.3 (CH), 129.7 (CH), 128.2 (C), 127.8 (C), 126.4 (CH), 123.8 (CH), 122.9 (CH), 121.8 (CH), 121.3 (CH), 121.0 (CH), 120.1 (CN), 58.2 (C), 39.8 (CH).

*5.1.1.4. 2-Amino-4-(2-bromophenyl)-4H-pyrano[3,2-h]quinoline-3-carbonitrile (**1d**).* Yield: 89%; mp 230-1 °C; IR (KBr) ν_{max} 2196 (CN), 3395, 3320 (NH_2) cm^{-1}; ^1H NMR (300 MHz, DMSO-d_6) δ 9.00-7.09 (m, 9Harom), 5.22 (br s, 2H, NH_2), 4.89 (s, H_{pyran}); ^{13}C NMR (75 MHz, DMSO-d_6) δ 159.4 (C), 156.8 (C), 150.5 (C), 143.3 (C), 137.9 (C), 136.3 (CH), 135.2 (CH), 131.6 (CH), 129.6 (C), 128.3 (C), 127.0 (CH), 126.9 (CH), 125.2 (CH), 122.1 (CH), 121.6 (CH), 121.1 (CH), 119.4 (CN), 59.8 (C), 41.2 (CH).

*5.1.1.5. 2-Amino-4-(4-nitrophenyl)-4H-pyrano[3,2-h]quinoline-3-carbonitrile (**1e**).* Yield: 77%; mp 230-1 °C; IR (KBr) ν_{max} 2196 (CN), 3395, 3320 (NH_2) cm^{-1}; ^1H NMR (300 MHz, DMSO-d_6) δ 9.00-7.09 (m, 9Harom), 5.22 (br s, 2H, NH2), 4.89 (s, H_{pyran}); ^{13}C NMR (75 MHz, DMSO-d_6) δ 165.1 (C), 154.3 (C), 152.1 (C), 150.6 (C), 142.5 (C), 138.4 (CH), 136.3

(C), 135.7 (CH), 134.5 (C), 131.4 (C), 129.1 (CH), 128.3 (CH), 127.5 (CH), 126.4 (CH), 124.5 (CH), 123.1 (CH), 122.7 (CN), 59.3 (C), 37.8 (CH).

*5.1.1.6. 2-Amino-4-(2,6-dichlorophenyl)-4H-pyrano[3,2-h]quinoline-3-carbonitrile (**1f**).* Yield: 87%; mp 244-5 °C; IR (KBr) ν_{max} 2190 (CN), 3390, 3330 (NH_2) cm^{-1}; ^1H NMR (300 MHz, DMSO-d_6) δ 9.06-7.11 (m, 8Harom), 5.26 (br s, 2H, NH_2), 4.93 (s, H_{pyran}); ^{13}C NMR (75 MHz, DMSO-d_6) δ 161.2 (C), 158.8 (C), 157.6 (C), 151.5 (C), 144.3 (C), 136.4 (C), 136.0 (CH), 135.2 (C), 131.2 (CH), 129.5 (C), 128.1 (CH), 127.6 (CH), 125.4 (CH), 122.8 (C), 121.6 (CH), 121.0 (CH), 119.8 (CN), 59.1 (C), 40.7 (CH).

*5.1.1.7. 2-Amino-4-(2-methoxyphenyl)-4H-pyrano[3,2-h]quinoline-3-carbonitrile (**1g**).* Yield: 88%; mp 217-9 °C; IR (KBr) ν_{max} 2217 (CN), 3436, 3320 (NH_2) cm^{-1}; ^1H NMR (300 MHz, DMSO-d_6) δ 8.90-7.33 (m, 9Harom), 7.21 (br s, 2H, NH_2), 5.28 (s, H_{pyran}), 3.77 (s, 3H, OCH_3); ^{13}C NMR (75 MHz, DMSO-d_6) δ 161.4 (C), 153.2 (C), 147.6 (C), 143.7 (C), 137.8 (CH), 136.7 (C), 134.1 (CH), 129.8 (CH), 128.1 (CH), 127.6 (CH), 126.9 (CH), 123.7 (CH), 123.1 (C), 122.1 (CH), 121.7 (CH), 121.0 (CH), 120.1 (CN), 56.3 (C), 55.5 (OCH_3), 40.4 (CH).

*5.1.1.8. 2-Amino-4-(3-methoxyphenyl)-4H-pyrano[3,2-h]quinoline-3-carbonitrile (**1h**).* Yield: 87%; mp 219-220 °C; IR (KBr) ν_{max} 2217 (CN), 3430, 3321 (NH_2) cm^{-1}; ^1H NMR (300 MHz, DMSO-d_6) δ 8.93-7.29 (m, 9Harom), 7.16 (br s, 2H, NH_2), 5.28 (s, H_{pyran}), 3.78 (s, 3H, OCH_3); ^{13}C NMR (75 MHz, DMSO-d_6) δ 161.9 (C), 155.9 (C), 149.8 (C), 143.7 (C), 137.8 (C), 136.1 (CH), 134.3 (C), 129.2 (CH), 128.5 (CH), 127.4 (CH), 126.9 (CH), 123.9 (CH), 122.9 (CH), 121.6 (CH), 121.0 (CH), 121.3 (CH), 119.8 (CN), 57.3 (C), 49.7 (OCH_3), 39.8 (CH).

*5.1.1.9. 2-Amino-4-(4-methoxyphenyl)-4H-pyrano[3,2-h]quinoline-3-carbonitrile (**1i**).* Yield: 90%; mp 217-9 °C; IR (KBr) ν_{max} 2222 (CN), 3430, 3330 (NH_2) cm^{-1}; ^1H NMR (300 MHz, DMSO-d_6) δ 8.95-7.33 (m, 9Harom), 7.20 (br s, 2H, NH_2), 4.90 (s, H_{pyran}), 3.70 (s, 3H,

OCH_3); ^{13}C NMR (75 MHz, DMSO-d_6) δ 161.4 (C), 156.8 (C), 150.5 (C), 143.7 (C), 137.8 (C), 136.4 (CH), 133.7 (C), 129.5 (CH), 128.8 (CH), 128.0 (CH), 126.9 (CH), 123.9 (CH), 122.8 (C), 122.6 (CH), 122.4 (CH), 121.3 (CH), 121.1 (CN), 56.3 (C), 53.7 (OCH_3), 41.7 (CH).

*5.1.1.10. 2-Amino-4-(p-tolyl)-4H-pyrano[3,2-h]quinoline-3-carbonitrile (**1j**).* Yield: 82%; mp 219-220 °C; IR (KBr) ν_{max} 2200 (CN), 3420, 3300 (NH_2) cm^{-1}; ^1H NMR (300 MHz, DMSO-d_6) δ 9.02-7.38 (m, 9Harom), 7.16 (br s, 2H, NH_2), 5.04 (s, H_{pyran}), 2.41 (s, 3H, CH_3); ^{13}C NMR (75 MHz, DMSO-d_6) δ 160.6 (C), 150.6 (C), 146.1 (C), 143.3 (C), 137.8 (CH), 136.4 (CH), 135.6 (CH), 133.5 (C), 129.1 (C), 128.1 (CH), 127.4 (CH), 127.3 (C), 123.9 (CH), 122.5 (CH), 122.3 (CH), 121.4 (CH), 120.8 (CN), 56.2 (C), 41.1 (CH), 28.6 (CH_3).

*5.1.1.11. 2-Amino-4-(pyridin-4-yl)-4H-pyrano[3,2-h]quinoline-3-carbonitrile (**1k**).* Yield: 81%; mp 196-8 °C; IR (KBr) ν_{max} 2225 (CN), 3526, 3445 (NH_2) cm^{-1}; ^1H NMR (300 MHz, DMSO-d_6) δ 8.94-7.22 (m, 9Harom), 7.12 (br s, 2H, NH_2), 4.95 (s, H_{pyran}); ^{13}C NMR (75 MHz, DMSO-d_6) δ 160.7 (C), 150.6 (C), 145.8 (C), 143.3 (C), 137.6 (C), 136.4 (CH), 133.1 (C), 129.1 (CH), 128.6 (C), 127.2 (CH), 126.5 (CH), 122.8 (CH), 122.4 (CH), 122.3 (CH), 121.6 (CH), 120.8 (CN), 57.2 (C), 39.9 (CH).

*5.1.1.12. 2-Amino-4-(2-bromopyridin-3-yl)-4H-pyrano[3,2-h]quinoline-3-carbonitrile (**1l**).* Yield: 81%; mp 232-3 °C; IR (KBr) ν_{max} 2196 (CN), 3395, 3320 (NH_2) cm^{-1}; ^1H NMR (300 MHz, DMSO-d_6) δ 8.97-7.11 (m, 8Harom), 5.17 (br s, 2H, NH_2), 4.77 (s, H_{pyran}); ^{13}C NMR (75 MHz, DMSO-d_6) δ 159.4 (C), 156.6 (C), 150.5 (C), 143.3 (C), 137.7 (C), 136.3 (C), 135.1 (CH), 131.5 (CH), 129.8 (CH), 128.3 (CH), 127.1 (CH), 126.9 (CH), 122.5 (CH), 121.6 (CH), 121.0 (CN), 59.2 (C), 39.6 (CH).

*5.1.2. General procedure for the of compounds **2a-l**.*

The 2-amino-4-aryl-4*H*-pyrano[3,2-h]quinoline-3-carbonitrile (1.0 equiv) was dissolved in distilled 1,4-dioxane (30 mL), and $AlCl_3$ (1.5 equiv) and cyclohexanone (1.5 equiv) were

added to this solution. The reaction mixture was heated at 110 °C for 2 h. When the reaction was complete (TLC analysis, CH_2Cl_2/EtOH, 10/1, v/v), the reaction mixture was diluted with a solution of dichloromethane/water (1/1), and treated with an aqueous solution of sodium hydroxide (10%) until pH 11-12. After stirring for 30 min, the mixture was extracted with CH_2Cl_2, dried over anhydrous sodium sulfate, filtered and the solvent was evaporated. The solid obtained washed with ether and filtered give pure product.

*5.1.2.1. 7-Phenyl-9,10,11,12-tetrahydro-7H-pyrano[2,3-b:5,6-h']diquinolin-8-amine (**2a**).*

Following the general method, reaction of compound **1a** (0.5 g, 1.6 mmol) in 1,4-dioxane (30 mL) with cyclohexanone (0.23 g, 2.4 mmol) and $AlCl_3$ (0.31 g, 2.4 mmol), after 2 h, product **2a** (0.6 g) was obtained: yield: 95%; mp >260 ºC; IR (KBr) ν_{max} 3333, 1517 cm^{-1}; ^{1}H NMR (300 MHz, DMSO-d_6) δ 8.94 (d, 1H, *J* = 8.4 Hz), 8.27 (d, 1H, *J*= 7.8 Hz), 7.56 (d, 2H, *J*= 8.4 Hz), 7.39-7.11 (m, 6Harom), 5.63 (br s, 2H, NH_2), 5.54 (s, 1H), 2.65-2.60 (m, 2H), 2.32-2.28 (m, 1H), 2.27-2.18 (m, 1H), 1.76-1.73 (m, 4H); ^{13}C NMR (75 MHz, DMSO-d_6) δ 155.7 (C), 153.3 (C), 153.0 (C), 151.9 (CH), 150.6 (C), 150.4 (C), 145.7 (C), 138.8 (CH), 129.0 (2 CH), 128.0 (CH), 127.9 (2 CH), 127.8 (C), 123.7 (C), 122.8 (C), 122.2 (CH), 121.9 (CH), 112.9 (CH), 112.7 (CH), 98.4 (C), 35.2 (CH), 32.6 (CH_2), 23.5 (CH_2), 22.8 (CH_2), 22.5 (CH_2). Anal. Calcd. for $C_{25}H_{21}N_3O.H_2O$: C, 75.55; H, 5.83; N, 10.57. Found: C, 75.26; H, 5.86; N, 10.57.

*5.1.2.2. 7-(2-Fluorophenyl)-9,10,11,12-tetrahydro-7H-pyrano[2,3-b:5,6-h']diquinolin-8-amine (**2b**).*

Following the general method, reaction of compound **1b** (0.5 g, 1.5 mmol) in 1,4-dioxane (30 mL) with cyclohexanone (0.22 g, 2.2 mmol) and $AlCl_3$ (0.29 g, 2.2 mmol), after 2 h, product **2b** (0.56 g) was obtained: yield: 90%; mp >260 ºC; IR (KBr) ν_{max} 3328, 1586 cm^{-1}; ^{1}H NMR (300 MHz, DMSO-d_6) δ 8.94 (d, 1H, *J*= 8.1 Hz), 8.29 (d, 1H, *J*= 7.8 Hz), 7.57-7.10 (m, 7H arom), 5.75 (s, 1H), 5.46 (br s, 2H, NH_2), 2.64-2.60 (m, 2H), 2.38-2.34 (m, 1H), 2.28-2.25 (m, 1H), 1.76-1.72 (m, 4H); ^{13}C NMR (100 MHz, DMSO-d_6) δ 159.1 (C), 155.9 (C), 153.4 (C),

151.8 (C), 150.4 (CH), 146.3 (C), 138.8 (C), 136.2 (CH), 131.6 (C), 130.6 (CH), 129.4 (CH), 128.3 (C), 127.3 (CH), 125.2 (CH), 122.6 (CH), 122.4 (CH), 121.6 (C), 116.5 (CH), 113.1 (C), 97.0 (C), 35.2 (CH), 32.7 (CH_2), 23.4 (CH_2), 22.9 (CH_2), 22.6 (CH_2). Anal. Calcd. for $C_{25}H_{20}FN_3O.H_2O$: C, 72.27; H, 5.34; N, 10.11. Found: C, 72.10; H, 5.23; N, 9.96.

*5.1.2.3. 7-(3-Fluorophenyl)-9,10,11,12-tetrahydro-7H-pyrano[2,3-b:5,6-h']diquinolin-8-amine (**2c**).*

Following the general method, reaction of compound **1c** (0.5 g, 1.5 mmol) in 1,4-dioxane (30 mL) with cyclohexanone (0.22 g, 2.2 mmol) and $AlCl_3$ (0.29 g, 2.2 mmol), after 2 h, product **2c** (0.58 g) was obtained: yield: 93%; mp >260 ºC; IR (KBr) ν_{max} 3331, 1592 cm^{-1} ; ^{1}H NMR (300 MHz, DMSO-d_6) δ 8.95 (d, 1H, *J*= 8.3 Hz), 8.30 (d, 1H, *J*= 7.8 Hz), 7.57 (d, 2H, *J*= 8.1 Hz), 7.42-6.94 (m, 5Harom), 5.71 (br s, 2H, NH_2), 5.59 (s, 1H), 3.56-3.50 (m, 2H), 2.36-2.32 (m, 1H), 2.23-2.20 (m, 1H), 1.76-1.73 (m, 4H); ^{13}C NMR (100 MHz, DMSO-d_6) δ 163.8 (C), 161.4 (C), 155.9 (C), 153.4 (C), 151.9 (C), 150.5 (CH), 148.4 (C), 138.9 (C), 136.2 (CH), 131.1 (CH), 128.3 (C), 127.4 (CH), 124.0 (CH), 123.1 (C), 122.9 (CH), 122.4 (CH), 114.6 (CH), 113.8 (CH), 113.8 (C), 98.1 (C), 32.7 (CH_2), 23.4 (CH_2), 22.9 (CH_2), 22.6 (CH_2). Anal. Calcd. for $C_{25}H_{20}FN_3O.H_2O$: C, 72.27; H, 5.34; N, 10.11. Found: C, 71.94; H, 5.30; N, 9.98.

Calcd. for $C_{25}H_{20}FN_3O.H_2O$: C, 72.27; H, 5.34; N, 10.11. Found: C, 71.94; H, 5.30; N, 9.98.

*5.1.2.4. 7-(2-Bromophenyl)-9,10,11,12-tetrahydro-7H-pyrano[2,3-b:5,6-h']diquinolin-8-amine (**2d**).*

Following the general method, reaction of compound **1d** (0.5 g, 1.3 mmol) in 1,4-dioxane (30 mL) with cyclohexanone (0.19 g, 1.95 mmol) and $AlCl_3$ (0.25 g, 1.95 mmol), after 2 h, product **2d** (0.60 g) was obtained: yield: 89%; mp >260 ºC; IR (KBr) ν_{max} 3312, 1591 cm^{-1}; ^{1}H NMR (300 MHz, DMSO-d_6) δ 8.95 (d, 1H, *J*= 8.1 Hz), 8.29 (d, 1H, *J*= 7.8 Hz), 7.59 (d, 2H, *J*= 8.4 Hz), 7.62-7.13 (m, 5Harom), 5.83 (s, 1H), 5.16 (br s, 2H, NH_2), 2.64-2.60 (m, 2H), 2.31-2.28 (m, 1H), 2.28-2.19 (m, 1H), 1.77-1.73 (m, 4H); ^{13}C NMR (100 MHz, DMSO-d_6) δ

155.5 (C), 153.8 (C), 151.7 (C), 150.5 (CH), 145.6 (C), 144.5 (C), 138.9 (C), 136.2 (CH), 133.3 (CH), 136.7 (CH), 129.7 (CH), 129.6 (CH), 128.4 (C), 122.9 (CH), 122.5 (CH), 122.0 (C), 121.8 (C), 113.3 (C), 98.9 (C), 32.7 (CH_2), 23.4 (CH_2), 22.8 (CH_2), 22.6 (CH_2). Anal. Calcd. for $C_{25}H_{20}BrN_3O.H_2O$: C, 63.03; H, 4.66; N, 8.82. Found: C, 62.85; H, 4.55; N, 8.85.

*5.1.2.5. 7-(4-Nitrophenyl)-9,10,11,12-tetrahydro-7H-pyrano[2,3-b:5,6-h']diquinolin-8-amine (**2e**).*

Following the general method, reaction of compound **1e** (0.5 g, 1.4 mmol) in 1,4-dioxane (30 mL) with cyclohexanone (0.19 g, 1.96 mmol) and $AlCl_3$ (0.26 g, 1.96 mmol), after 2 h, product **2e** (0.55 g) was obtained: yield: 90%; mp >260 ºC; IR (KBr) ν_{max} 3311, 1597 cm^{-1}; ^1H NMR (300 MHz, DMSO-d_6) δ 8.95 (d, 1H, *J*= 8.4 Hz), 8.27 (d, 1H, *J*= 7.8 Hz), 7.90 (d, 2H *J*= 8.4 Hz), 7.57-7.12 (m, 5Harom), 5.91 (s, 1H), 5.57 (br s, 2H, NH_2), 2.66-2.62 (m, 2H), 2.33-2.29 (m, 1H), 2.28-2.20 (m, 1H), 1.77-1.73 (m, 4H); ^{13}C NMR (100 MHz, DMSO-d_6) δ 155.7 (C), 154.0 (C), 152.0 (C), 150.7 (CH), 148.8 (C), 145.6 (C), 138.8 (C), 138.5 (C), 136.3 (CH), 134.6 (2 CH), 131.4 (CH), 129.6 (CH), 128.4 (C), 126.6 (CH), 124.3 (CH), 123.2 (CH), 122.7 (CH), 121.4 (C), 113.3 (C), 97.0 (C), 35.6 (CH), 32.7 (CH_2), 23.4 (CH_2), 22.8 (CH_2), 21.5 (CH_2). Anal. Calcd. for $C_{25}H_{20}N_4O_3.H_2O$: C, 67.86; H, 5.01; N, 12.66. Found: C, 68.02; H, 4.88; N, 12.61.

*5.1.2.6. 7-(2,6-Dichlorophenyl)-9,10,11,12-tetrahydro-7H-pyrano[2,3-b:5,6-h']diquinolin-8-amine (**2f**).*

Following the general method, reaction of compound **1f** (0.5 g, 1.3 mmol) in 1,4-dioxane (30 mL) with cyclohexanone (0.19 g, 1.95 mmol) and $AlCl_3$ (0.25 g, 1.95 mmol), after 2 h, product **2f** (0.56 g) was obtained: yield: 92%; mp >260 ºC; IR (KBr) ν_{max} 3332, 1590 cm^{-1}; ^1H NMR (300 MHz, DMSO-d_6) δ 8.94 (d, 1H, *J*= 8.4 Hz), 8.29 (d, 1H, *J*= 7.8 Hz), 7.69 (d, 2H, *J*= 8.4 Hz), 7.60-7.08 (m, 4Harom), 5.90 (s, 1H), 5.59 (br s, 2H, NH_2), 2.65-2.61 (m, 2H), 2.32-2.29 (m, 1H), 2.27-2.22 (m, 1H), 1.76-1.73 (m, 4H); ^{13}C NMR (100 MHz, DMSO-d_6) δ

155.9 (C), 153.6 (C), 151.6 (C), 150.5 (CH), 146.8 (C), 138.4 (C), 137.7 (C), 130.7 (2xCH), 128.6 (2xC), 126.1 (CH), 122.5 (CH), 117.9 (C), 113.2 (C), 95.6 (C), 37.6 (CH), 32.6 (CH_2), 23.3 (CH_2), 22.8 (CH_2), 22.6 (CH_2). Anal. Calcd. for $C_{25}H_{19}Cl_2N_3O.2H_2O$: C, 61.99; H, 4.79; N, 8.68. Found: C, 62.09; H, 4.64; N, 8.46.

*5.1.2.7. 7-(2-Methoxyphenyl)-9,10,11,12-tetrahydro-7H-pyrano[2,3-b:5,6-h']diquinolin-8-amine (**2g**).*

Following the general method, reaction of compound **1g** (0.5 g, 1.5 mmol) in 1,4-dioxane (30 mL) with cyclohexanone (0.22 g, 2.25 mmol) and $AlCl_3$ (0.29 g, 2.25 mmol), after 2 h, product **2g** (0.57 g) was obtained: yield: 92%; mp >260 ºC; IR (KBr) ν_{max} 3307, 1589 cm^{-1}; ^1H NMR (300 MHz, DMSO-d_6) δ 8.94 (d, 1H, *J*= 8.3 Hz), 8.30 (d, 1H, *J*= 7.8 Hz), 7.56 (d, 2H, *J*= 8.1 Hz), 7.27-6.82 (m, 5Harom), 5.73 (s, 1H), 5.36 (br s, 2H, NH_2), 3.92 (s, 3H, OCH_3), 3.57-3.50 (m, 2H), 2.65-2.61 (m, 2H), 2.33-2.29 (m, 1H), 2.26-2.22 (m, 1H), 1.76-1.73 (m, 2H); ^{13}C NMR (75 MHz, DMSO-d_6) δ 155.5 (C), 155.8 (C), 153.1 (C), 152.9 (C), 150.4 (CH), 147.2 (C), 145.7 (C), 138.8 (C), 136.2 (CH), 130.2 (CH), 128.1 (C), 127.4 (CH), 123.8 (C), 122.7 (CH), 122.6 (CH), 120.2 (CH), 114.5 (CH), 112.8 (C), 111.6 (CH), 98.4 (C), 53.2 (OCH_3), 32.5 (CH), 23.3 (CH_2), 22.8 (CH_2), 22.7 (CH_2), 22.4 (CH_2). Anal. Calcd. for $C_{26}H_{23}N_3O_2.2H_2O$: C, 70.09; H, 6.11; N, 9.43. Found: C, 70.13; H, 5.91; N, 9.20.

*5.1.2.8. 7-(3-Methoxyphenyl)-9,10,11,12-tetrahydro-7H-pyrano[2,3-b:5,6-h']diquinolin-8-amine (**2h**).*

Following the general method, reaction of compound **1h** (0.5 g, 1.5 mmol) in 1,4-dioxane (30 mL) with cyclohexanone (0.22 g, 2.25 mmol) and $AlCl_3$ (0.29 g, 2.25 mmol), after 2 h, product **2h** (0.57 g) was obtained: yield: 93%; mp >260 ºC; IR (KBr) ν_{max} 3327, 1596 cm^{-1}; ^1H NMR (300 MHz, DMSO-d_6) δ 8.94 (d, 1H, *J*= 8.3 Hz), 8.30 (d, 1H, *J*= 7.8 Hz), 7.58 (m, 2H), 7.39 (d, 1H, *J*= 7.8 Hz), 7.16 (d, 2H, *J*= 8.9 Hz), 6.71 (d, 2H, *J*= 8.7 Hz), 5.62 (br s, 2H, NH_2), 5.49 (s, 1H), 3.68 (s, 3H, OCH_3), 2.64-2.60 (m, 2H), 2.54-2.50 (m, 2H), 2.35-2.31(m,

1H), 2.29-2.26 (m, 1H), 1.76-1.73 (m, 2H); ^{13}C NMR (75 MHz, DMSO-d_6) δ 159.7 (C), 155.8 (C), 153.1 (C), 151.8 (C), 150.4 (CH), 147.2 (C), 145.7 (C), 138.8 (C), 136.2 (CH), 130.2 (CH), 128.1 (C), 127.4 (CH), 123.5 (C), 122.7 (CH), 122.2 (CH), 120.2 (CH), 114.5 (CH), 112.8 (C), 111.6 (CH), 98.3 (C), 55.4 (OCH_3), 32.6 (CH), 23.4 (CH_2), 22.8 (CH_2), 22.7 (CH_2), 22.6 (CH_2). Anal. Calcd. for $C_{26}H_{23}N_3O_2.2H_2O$: C, 70.09; H, 6.11; N, 9.43. Found: C, 70.20; H, 6.02; N, 9.39.

*5.1.2.9. 7-(4-Methoxyphenyl)-9,10,11,12-tetrahydro-7H-pyrano[2,3-b:5,6-h']diquinolin-8-amine (**2i**).*

Following the general method, reaction of compound **1i** (0.5 g, 1.5 mmol) in 1,4-dioxane (30 mL) with cyclohexanone (0.22 g, 2.25 mmol) and $AlCl_3$ (0.29 g, 2.25 mmol), after 2 h, product **2i** (0.55 g) was obtained: yield: 89%; mp >260 ºC; IR (KBr) ν_{max} 3336, 1592 cm^{-1}; ^{1}H NMR (300 MHz, DMSO-d_6) δ 8.93 (d, 1H, *J*= 8.1 Hz), 8.28 (d, 1H, *J*= 7.8 Hz), 7.57 (m, 2H), 7.36 (d, 1H, *J*= 7.8 Hz), 7.25 (d, 2H, *J*= 8.9 Hz), 6.80 (d, 2H, *J*= 8.7 Hz), 5.58 (br s, 2H, NH_2), 5.46 (s, 1H), 3.64 (s, 3H, OCH_3), 2.65-2.60 (m, 2H), 2.54-2.51 (m, 2H), 2.44-2.39 (m, 1H), 2.36-2.32 (m, 1H), 1.78-1.75 (m, 2H); ^{13}C NMR (75 MHz, DMSO-d_6) δ 158.3 (C), 155.7 (C), 152.9 (C), 151.8 (C), 150.3 (C), 145.6 (CH), 138.8 (C), 136.2 (CH), 131.8 (C), 128.8 (2 CH), 128.0 (C), 127.6 (2 CH), 123.9 (C), 123.4 (C), 122.6 (CH), 114.3 (C), 112.8 (CH), 98.6 (C), 55.4 (OCH_3), 32.6 (CH), 26.6 (CH_2), 23.5 (CH_2), 23.1 (CH_2), 22.8 (CH_2). Anal. Calcd. for $C_{26}H_{23}N_3O_2.H_2O$: C, 73.05; H, 5.89; N, 9.83. Found: C, 73.19; H, 5.97; N, 9.60.

*5.1.2.10. 7-(p-Tolyl)-9,10,11,12-tetrahydro-7H-pyrano[2,3-b:5,6-h']diquinolin-8-amine (**2j**).*

Following the general method, reaction of compound **1j** (0.5 g, 1.6 mmol) in 1,4-dioxane (30 mL) with cyclohexanone (0.23 g, 2.4 mmol) and $AlCl_3$ (0.31 g, 2.4 mmol), after 2 h, product **2j** (0.56 g) was obtained: yield: 90%; mp >260 ºC; IR (KBr) ν_{max} 3300, 1597 cm^{-1}; ^{1}H NMR (300 MHz, DMSO-d_6) δ 8.93 (d, 1H, *J* = 8.2 Hz), 8.28 (d, 1H, *J*= 7.8 Hz), 7.55 (m, 2H), 7.35 (d, 1H, *J*= 7.8 Hz), 7.24 (d, 2H, *J*= 8.9 Hz), 7.02 (d, 2H, *J*= 8.7 Hz), 5.57 (br s, 2H, NH_2),

5.47 (s, 1H), 2.64-2.61 (m, 2H), 2.53-2.50 (m, 2H), 2.43-2.39 (m, 1H), 2.36-2.33 (m, 1H), 2.16 (s, 3H, CH_3), 1.76-1.72 (m, 2H); ^{13}C NMR (100 MHz, DMSO-d_6) δ 155.7 (C), 153.0 (C), 151.8 (C), 150.3 (CH), 145.6 (C), 142.8 (C), 138.8 (C), 136.2 (C), 131.8 (CH), 129.6 (CH), 128.0 (2 CH), 127.8 (C), 127.5 (2 CH), 123.7 (C), 122.6 (CH), 122.2 (CH), 112.8 (C), 98.6 (C), 39.8 (CH), 32.6 (CH_2), 23.4 (CH_2), 22.8 (CH_2), 22.6 (CH_2), 20.9 (CH_3). Anal. Calcd. for $C_{26}H_{23}N_3O.H_2O$: C, 75.89; H, 6.12; N, 10.21. Found: C, 76.02; H, 5.96; N, 10.07.

*5.1.2.11. 7-(Pyridin-4-yl)-9,10,11,12-tetrahydro-7H-pyrano[2,3-b:5,6-h']diquinolin-8-amine (**2k**).*

Following the general method, reaction of compound **1k** (0.5 g, 1.3 mmol) in 1,4-dioxane (30 mL) with cyclohexanone (0.19 g, 1.95 mmol) and $AlCl_3$ (0.25 g, 1.95 mmol), after 2 h, product **2k** (0.55 g) was obtained: yield: 87%; mp >260 ºC; IR (KBr) ν_{max} 3302, 1591 cm^{-1}; ^{1}H NMR (300 MHz, DMSO-d_6) δ 8.93 (d, 1H, *J*= 8.1 Hz), 8.27 (d, 1H, *J*= 7.8 Hz), 7.67 (d, 2H, *J*= 8.4 Hz), 7.62-7.07 (m, 5Harom), 5.92 (s, 1H), 5.59 (s, 2H, NH_2), 2.64-2.61 (m, 2H), 2.32-2.29 (m, 1H), 2.29-2.24 (m, 1H), 1.76-1.72 (m, 4H); ^{13}C NMR (75 MHz, DMSO-d_6) δ 155.8 (C), 153.7 (C), 153.5 (C), 152.0 (C), 150.6 (CH), 150.3 (C), 148.6 (C), 147.2 (CH), 146.1 (C), 138.7 (CH), 136.3 (CH), 128.3 (2 CH), 123.1 (2 CH), 122.5 (C), 122.2 (C), 97.1 (C), 38.1 (CH), 32.6 (CH_2), 23.5 (CH_2), 22.8 (CH_2), 22.5 (CH_2). Anal. Calcd. for $C_{24}H_{20}N_4O.H_2O$: C, 72.34; H, 5.57; N, 14.06. Found: C, 72.59; H, 5.38; N, 13.88.

*5.1.2.12. 7-(2-Bromopyridin-3-yl)-9,10,11,12-tetrahydro-7H-pyrano[2,3-b:5,6-h']diquinolin-8-amine (**2l**).*

Following the general method, reaction of compound **1l** (0.5 g, 1.3 mmol) in 1,4-dioxane (30 mL) with cyclohexanone (0.19 g, 1.95 mmol) and $AlCl_3$ (0.25 g, 1.95 mmol), after 2 h, product **2l** (0.49 g) was obtained: yield: 81%; mp >260 ºC; IR (KBr) ν_{max} 3317, 1597 cm^{-1}; ^{1}H NMR (300 MHz, DMSO-d_6) δ 8.96 (d, 1H, *J*= 8.1 Hz), 8.31 (d, 1H, *J*= 7.8 Hz), 7.60 (d, 2H, *J*= 8.4 Hz), 7.39-6.92 (m, 4Harom), 5.84 (s, 1H), 5.25 (br s, 2H, NH_2), 2.39-2.36 (m, 2H),

2.33-2.29 (m, 1H), 2.26-2.19 (m, 1H), 1.77-1.73 (m, 4H); ^{13}C NMR (100 MHz, DMSO-d_6) δ 155.5 (C), 154.1 (C), 151.8 (C), 150.6 (CH), 149.7 (CH), 145.8 (C), 141.7 (C), 141.4 (C), 140.4 (CH), 138.9 (C), 136.3 (CH), 128.6 (C), 126.4 (CH), 125.3 (CH), 123.1 (CH), 122.7 (CH), 120.9 (C), 113.5 (C), 97.5 (C), 32.7 (CH_2), 23.4 (CH_2), 22.8 (CH_2), 22.5 (CH_2). Anal. Calcd. for $C_{24}H_{19}BrN_4O.H_2O$: C, 60.39; H, 4.43; N, 11.74. Found: C, 60.51; H, 4.38; N, 11.79.

5.2. Antioxidant test: Oxygen Radical Absorbance Capacity Assay

The antioxidant activity of compounds **2a-l** was determined by the oxygen radical absorbance capacity-fuorescein (ORAC-FL) method [26,27] using 2,2'-azobis(amidinopropane) dihydrochloride (AAPH) as generator of peroxyl radicals at 37 °C. The reaction mixture was carried out at 37 °C in 75 mM phosphate buffer (pH 7.4). Firstly a solution made up of antioxidant (20 µL) and fluorescein (FL, 120 µL, final concentration of 70 nM) were incubated in a black 96-well microplate (Nunc) for 15 min at 37 °C into a Varioskan Flash plate reader with built-in injectors (Thermo Scientific). Then, 2,2'-azobis(amidinopropane) dihydrochloride (AAPH, 60 µL, final concentration of 12 mM) solution was added quickly using the built-in injector and the fluorescence was measured every minute for 60 min at λ_{ex}= 485 nm and λ_{em}= 535 nm. The blank was composed of 120 µL of FL, 60 µL of AAPH and 20 µL of phosphate buffer (pH= 7.4) was carried out in each assay. The Trolox was used as standard with 1–8 µM as final concentration and the samples were measured at different concentrations 0.1–1 µM. All assays were run in triplicate and at least three different assays were conducted for each sample. Fluorescence measurement was first normalized to the curve of the blank (without antioxidant and the area under the fluorescence decay curve (AUC) was calculated as: AUC= 1 + sum(fi/f_0),

Where f_0 is the initial fluorescence at 0 min and f_i is the fluorescence at time *i*. The net AUC for each the sample was calculated as follows:

Net AUC= $AUC_{antioxidant} - AUC_{blank}$.

The regression equations were extrapolated by plotting the net AUC against the concentration of the antioxidant. The ORAC values correspond to the ratio of slopes of the latter curve and Trolox in the same assay. Final ORAC values were expressed as Trolox equivalents and data are expressed as means±SD.

5.3. Studies of metal-chelating properties [36,37]

The metal binding studies were performed with a UV GBC CINTRA spectrophotometer. The UV absorption spectra of compound **2h** in the absence or presence of different amount of $CuSO_4$, and $FeSO_4$ were recorded with wavelength ranging from 200 to 400 nm after incubating for 30 min and 20 h at room temperature. The final volume of reaction mixture was 1 mL, the final concentrations of tested compound 10 μM and the 4 or 5 final concentrations of biometal ranging from 0 to 20 μM.

5.4. Inhibition of EeAChE and eqBuChE

Ellman's assay was followed to assess the anticholinesterasic activity of **2a-l** [25] using purified AChE from *Electrophorus electricus* (Type V-S, Sigma-Aldrich) or BuChE from horse serum (lyophilized powder, Sigma-Aldrich). Enzymatic reaction was performed in a final volume of 3 mL containing 0.1 M phosphate-buffered at pH 8.0, 0.035 U/mL *Ee*AChE or 0.05 U/mL, 0.35 mM of 5,5'-dithiobis-2-nitrobenzoic acid (DTNB) and 40 μL of Bovine Albumin Serum (BSA) 1% (w/v) in phosphate-buffered at pH 8.0. Inhibition curves were plotted by pre-incubating this blend with nine concentrations of each compound for 10 min. The activity in absence of compound was used as control. Then, the substrate was added to a

final concentration of 0.35 mM for acetylthiocholine iodide and 0.5 mM for butyrylthiocholine iodide and incubated for another 15 min at rt. Changes in absorbance at 412 nm were measured in a spectrometric plate reader (iEMS Reader MF, Labsystems). The IC_{50} values were calculated using GraphPad Prism 5. Data is expressed as mean±SEM at least three different experiments.

5.5. Inhibition of hAChE

Evaluation of the inhibitory potency of compounds **2a-l** was carried out following the spectrophotometric Ellman's method [25] using human recombinant AChE (Sigma–Aldrich). The assay was performed in 0.1 M phosphate buffer pH 8.0. First the tested compounds or blank (water) (25 µL) were incubated with 20 µL of the enzyme (5 U/mL) for 5 min at 37 °C in 765 µL of phosphate buffer. Then, 20 µL of 12.5 mM of 5,5'-dithiobis-(2-nitrobenzoic acid) DTNB solution containing 0.15% (w/v) sodium carbonate and 20 µL of ATC (18.75 mM) were added and incubated for 5 min. The absorbance variation was measured at 412 nm with EnSpire Multimode microplate reader (PerkinElmer). IC_{50} values were determined with GraphPad Prism 5. Each concentration was measured in triplicate. Data is expressed as mean±SEM.

5.6. Cholinesterase inhibition kinetic assessment

To estimate the mechanism of inhibition of **2h**, the same experimental protocol [25] as reported for *h*AChE inhibition was performed. All experiments were performed in triplicate. Reciprocal plots of 1/V versus 1/[S] were determined using concentrations of inhibitor ranging (0.30–3.0 µM) and concentrations of substrate ATC ranging (0.067-0.5 mM). The double reciprocal plots were analysed by a weighted least square procedure that assumed the variance of *V* to be constant. Cornish-Bowden plots obtained by plotting S/*V* (substrate/velocity ratio) versus the inhibitor concentration [25,38] were used to confirm the

mode of inhibition. Inhibitor constant (K_i) value was determined by re-plotting slopes from the Lineweaver-Burk plot versus the inhibitor concentration where K_i was determined as the intersect of the line with the x-axis [39] using GraphPad Prism 5.

*5.7. In vitro cytotoxicity of compounds **2a, 2c and 2h-j** in HepG2 cells*

HepG2 cells were purchased from American Type Culture Collection. The cells were cultured in Eagle's Minimum Essential Medium (Ozyme, France) supplemented with 10% fetal bovine serum, 1X non-essential amino acids, 100 units/mL penicillin and 10 mg/mL streptomycin (Dutscher, France). Cultures were kept under a CO_2/air (5%/95%) humidified atmosphere at 37 °C. Prior to the experiment, cells were seeded in 96-well culture plates at a density of 0.1×10^6 cells per well. After 24h of incubation, the culture medium was refreshed and 100 µl of the test compounds or DMSO (0.1%) were added. Compounds were tested at six concentrations (1-1000 µM) in triplicate. For the MTT assay [40], after 24h of treatment, cells were incubated with 50 µL MTT (0.5 mg/mL, Sigma Aldrich, France) at 37 °C for 2h. Plates were centrifuged, MTT was removed and 100 µL DMSO was distributed per well. The absorbance at 570 nm was measured using microplate reader (brand). Cell viability was expressed as percentage of cell viability compared to controls (DMSO, 0.1%).

*5.8 In vitro cytotoxicity of tacrine and **2h** in primary human hepatocytes*

The pool of cryopreserved primary human hepatocytes P0203T (n = 9 donors) was provided by KaLy-Cell (Plobsheim, France). The pooled hepatocytes were thawed in a water-bath (1 - 2 minutes) and diluted in 50 mL KLC-Thawing Medium (KLC-TM; proprietary formulation); centrifuged 170 x *g*; 20 minutes; room temperature, washed (KLC-Washing Medium (KLC-WM; proprietary formulation)); 100 x *g*; 5 min; room temperature and re-suspended in KLC-Suspension Medium (KLC-SuM; proprietary formulation). Cell number and viability were determined by the trypan blue exclusion method. After dilution to a concentration of 2 x

10^6 viable cells/mL in medium, the hepatocyte suspension was distributed into eight 96-well plates (50 µL/well). The plates were pre-incubated for approximately 15 min under shaking (900 rpm) in a humidified chamber at 37°C with 5% CO_2. Suspended hepatocytes (50 µL) were dosed in technical triplicates in serum-free medium with 50 µL of 2-fold concentrated tacrine or 2 h. Due to solubility limits in treatment medium, maximum tested concentrations were 100 µM for both compounds. During the incubation period of 2 h, the plates were shaken at 163 g in a humidified chamber at 37 °C with 5% CO_2 which has been shown to increase the metabolic performance of the cells.

5.9. PAMPA assay

Penetration across the BBB is an essential property for compounds targeting the CNS. In order to predict passive blood-brain penetration of novel compounds modification of the parallel artificial membrane permeation assay (PAMPA) has been used based on reported protocol [33]. The filter membrane of the donor plate was coated with PBL (Polar Brain Lipid, Avanti, USA) in dodecane (4 µL of 20 mg/mL PBL in dodecane) and the acceptor well was filled with 300 µl of PBS pH 7.4 buffer (V_D). Tested compounds were dissolved first in DMSO and that diluted with PBS pH 7.4 to reach the final concentration of 100 µM in the donor well. Concentration of DMSO did not exceed 0.5% (V/V) in the donor solution. The donor solution (300 µL) was added to the donor wells (V_A) and the donor filter plate was carefully put on the acceptor plate so that the coated membrane was “in touch” with both donor solution and acceptor buffer. Test compound diffused from the donor well through the lipid membrane (Area= 0.28cm^2) to the acceptor well. The concentration of the drug in both donor and the acceptor wells was assessed after 3, 4, 5 and 6 h of incubation in quadruplicate using the UV plate reader Synergy HT (Biotek, USA) at the maximum absorption wavelength

of each compound. Concentration of the compounds was calculated from the standard curve and expressed as the permeability (Pe) according the equation (1) [41,42]:

$$\log P_e = \log\left\{C \times -ln\left(1 - \frac{[drug]_{acceptor}}{[drug]_{equilibrium}}\right)\right\} \; where \; C = \left(\frac{V_D \times V_A}{(V_D + V_A) \times Area \times time}\right) (1)$$

5.10. Molecular modeling

Compounds (*R*)-**2h** and (*S*)-**2h** were assembled within Discovery Studio, version 2.1, software package, using standard bond lengths and bond angles. With the CHARMm force field [43] and partial atomic charges, the molecular geometries of (*R*)-**2h** and (*S*)-**2h** were energy-minimized using the adopted-based Newton-Rapson algorithm. Structure was considered fully optimized when the energy changes between interactions were less than 0.01 Kcal/mol [44].

The coordinates of hAChE complexed with fasciculin-II (PDB: 1B41), were obtained from the Protein Data Bank (PDB). For docking studies, initial protein was prepared by removing all water molecules, heteroatoms, any co-crystallized solvent and the ligand. Proper bonds, bond orders, hybridization and charges were assigned using protein model tool in Discovery Studio, version 2.1, software package. CHARMm force field was applied using the receptor-ligand interactions tool in Discovery Studio, version 2.1, software package. Docking calculations were performed with the program Autodock Vina [34]. AutoDockTools (ADT; version 1.5.4) was used to add hydrogens and partial charges for proteins and ligands using Gasteiger charges. A grid box with size of 60 x 60 x 72 with grid points separated 1 Å, was used in the configuration file of the Autodock Vina software to cover the entire enzyme. The grid box was centered at the coordinate of x = 116.546; y = 110.33; z = -134.181. Flexible torsions in the ligands were assigned with the AutoTors module, and the acyclic dihedral angles were allowed to rotate freely. Trp286, Tyr124, Tyr337, Tyr72, Asp74, Thr75, Trp86, Phe338, Phe297and Tyr341 receptor residues were selected to keep flexible during docking simulation using the AutoTors module. Other docking parameters were set to default except

num_modes, which was set to 40. The AutoDock Vina docking procedure used was previously validated [45]. Finally, the docking results generated were directly loaded into Discovery Studio, version 2.1.

5.11. DFT study

The structures of all the complexes and ligands under study were optimized using the Gaussian 09 program [46] at the DFT level of theory using the B3LYP exchange-correlation functional [47,48]. Regarding to the basis set, def2-tzvp has been selected for Cu and 6-311g(2d) for the rest of the atoms.

ACKNOWLEDGMENTS

L.I thanks the Regional Council of Franche-Comté for financial support. We also thank Mrs. M. Untrau and C parmentier from Kaly-ceell for their technical support in assessing cytotocicity towards primary human hepatocytes. O.S thanks MH CZ - DRO (UHHK 00179906)

References

[1] H.W. Querfurth, F.M. LaFerla, Alzheimer's Disease, N. Engl. J. Med. 362 (2010) 329–344. doi:10.1056/NEJMra0909142.
[2] M. Goedert, M.G. Spillantini, A century of Alzheimer's disease, Science. 314 (2006) 777–781. doi:10.1126/science.1132814.
[3] V.H. Finder, Alzheimer's disease: a general introduction and pathomechanism, J. Alzheimers Dis. JAD. 22 Suppl 3 (2010) 5–19. doi:10.3233/JAD-2010-100975.
[4] M.G. Savelieff, S. Lee, Y. Liu, M.H. Lim, Untangling Amyloid-β, Tau, and Metals in Alzheimer's Disease, ACS Chem. Biol. 8 (2013) 856–865. doi:10.1021/cb400080f.
[5] V. Tumiatti, A. Minarini, M.L. Bolognesi, A. Milelli, M. Rosini, C. Melchiorre, Tacrine derivatives and Alzheimer's disease, Curr. Med. Chem. 17 (2010) 1825–1838.
[6] X. Huang, R.D. Moir, R.E. Tanzi, A.I. Bush, J.T. Rogers, Redox-Active Metals, Oxidative Stress, and Alzheimer's Disease Pathology, Ann. N. Y. Acad. Sci. 1012 (2004) 153–163. doi:10.1196/annals.1306.012.
[7] A.I. Bush, Drug development based on the metals hypothesis of Alzheimer's disease, J. Alzheimers Dis. JAD. 15 (2008) 223–240.
[8] C. Opazo, X. Huang, R.A. Cherny, R.D. Moir, A.E. Roher, A.R. White, R. Cappai, C.L.

Masters, R.E. Tanzi, N.C. Inestrosa, A.I. Bush, Metalloenzyme-like Activity of Alzheimer's Disease -Amyloid: Cu-DEPENDENT CATALYTIC CONVERSION OF DOPAMINE, CHOLESTEROL, AND BIOLOGICAL REDUCING AGENTS TO NEUROTOXIC H2O2, J. Biol. Chem. 277 (2002) 40302–40308. doi:10.1074/jbc.M206428200.
[9] M. Bond, G. Rogers, J. Peters, R. Anderson, M. Hoyle, A. Miners, T. Moxham, S. Davis, P. Thokala, A. Wailoo, M. Jeffreys, C. Hyde, The effectiveness and cost-effectiveness of donepezil, galantamine, rivastigmine and memantine for the treatment of Alzheimer's disease (review of Technology Appraisal No. 111): a systematic review and economic model., Health Technol. Assess. 16 (2012). doi:10.3310/hta16210.
[10] D. Wilkinson, Y. Wirth, C. Goebel, Memantine in Patients with Moderate to Severe Alzheimer's Disease: Meta-Analyses Using Realistic Definitions of Response, Dement. Geriatr. Cogn. Disord. 37 (2014) 71–85. doi:10.1159/000353801.
[11] P.M. Weinstock, Selectivity of Cholinesterase Inhibition, CNS Drugs. 12 (2012) 307–323. doi:10.2165/00023210-199912040-00005.
[12] R. Morphy, Z. Rankovic, Designing Multiple Ligands – Medicinal Chemistry Strategies and Challenges, Curr. Pharm. Des. 15 (2009) 587–600. doi:10.2174/138161209787315594.
[13] A. Agis-Torres, M. Sollhuber, M. Fernandez, J.M. Sanchez-Montero, Multi-Target-Directed Ligands and other Therapeutic Strategies in the Search of a Real Solution for Alzheimer's Disease, Curr. Neuropharmacol. 12 (2014) 2–36. doi:10.2174/1570159X113116660047.
[14] A. Cavalli, M.L. Bolognesi, A. Minarini, M. Rosini, V. Tumiatti, M. Recanatini, C. Melchiorre, Multi-target-Directed Ligands To Combat Neurodegenerative Diseases, J. Med. Chem. 51 (2008) 347–372. doi:10.1021/jm7009364.
[15] R. León, A.G. Garcia, J. Marco-Contelles, Recent advances in the multitarget-directed ligands approach for the treatment of Alzheimer's disease, Med. Res. Rev. 33 (2013) 139–189. doi:10.1002/med.20248.
[16] A. Rampa, F. Belluti, S. Gobbi, A. Bisi, Hybrid-Based Multi-Target Ligands for the Treatment of Alzheimer's Disease, Curr. Top. Med. Chem. 11 (2011) 2716–2730. doi:10.2174/156802611798184409.
[17] L. Ismaili, B. Refouvelet, M. Benchekroun, S. Brogi, M. Brindisi, S. Gemma, G. Campiani, S. Filipic, D. Agbaba, G. Esteban, M. Unzeta, K. Nikolic, S. Butini, J. Marco-Contelles, Multitarget compounds bearing tacrine- and donepezil-like structural and functional motifs for the potential treatment of Alzheimer's disease, Prog. Neurobiol. (n.d.). doi:10.1016/j.pneurobio.2015.12.003.
[18] M. Benchekroun, L. Ismaili, M. Pudlo, V. Luzet, T. Gharbi, B. Refouvelet, J. Marco-Contelles, Donepezil–ferulic acid hybrids as anti-Alzheimer drugs, Future Med. Chem. 7 (2015) 15–21. doi:10.4155/fmc.14.148.
[19] M. Benchekroun, M. Bartolini, J. Egea, A. Romero, E. Soriano, M. Pudlo, V. Luzet, V. Andrisano, M.-L. Jimeno, M.G. López, S. Wehle, T. Gharbi, B. Refouvelet, L. de Andrés, C. Herrera-Arozamena, B. Monti, M.L. Bolognesi, M.I. Rodríguez-Franco, M. Decker, J. Marco-Contelles, L. Ismaili, Novel Tacrine-Grafted Ugi Adducts as Multipotent Anti-Alzheimer Drugs: A Synthetic Renewal in Tacrine-Ferulic Acid Hybrids, ChemMedChem. 10 (2015) 523–539. doi:10.1002/cmdc.201402409.
[20] I. Tomassoli, L. Ismaili, M. Pudlo, C. de los Ríos, E. Soriano, I. Colmena, L. Gandía, L. Rivas, A. Samadi, J. Marco-Contelles, B. Refouvelet, Synthesis, biological assessment and molecular modeling of new dihydroquinoline-3-carboxamides and dihydroquinoline-3-carbohydrazide derivatives as cholinesterase inhibitors, and Ca channel antagonists, Eur. J. Med. Chem. 46 (2011) 1–10. doi:10.1016/j.ejmech.2010.08.054.

[21] Z. Wang, W. Li, Y. Wang, X. Li, L. Huang, X. Li, Design, synthesis and evaluation of clioquinol–ebselen hybrids as multi-target-directed ligands against Alzheimer's disease, RSC Adv. 6 (2016) 7139–7158. doi:10.1039/C5RA26797H.
[22] Watkins PB, Zimmerman HJ, Knapp MJ, Gracon SI, Lewis KW, HEpatotoxic effects of tacrine administration in patients with alzheimer's disease, JAMA. 271 (1994) 992–998. doi:10.1001/jama.1994.03510370044030.
[23] Y. Dgachi, L. Ismaili, D. Knez, M. Benchekroun, H. Martin, N. Szałaj, S. Wehle, O.M. Bautista-Aguilera, V. Luzet, A. Bonnet, B. Malawska, S. Gobec, M. Chioua, M. Decker, F. Chabchoub, J. Marco-Contelles, Synthesis and Biological Assessment of Racemic Benzochromenopyrimidinimines as Antioxidant, Cholinesterase, and Aβ1−42 Aggregation Inhibitors for Alzheimer's Disease Therapy, ChemMedChem. (2016) n/a-n/a. doi:10.1002/cmdc.201500539.
[24] J. Marco-Contelles, E. Pérez-Mayoral, A. Samadi, M. do C. Carreiras, E. Soriano, Recent Advances in the Friedländer Reaction, Chem. Rev. 109 (2009) 2652–2671. doi:10.1021/cr800482c.
[25] G.L. Ellman, K.D. Courtney, V. Andres jr., R.M. Featherstone, A new and rapid colorimetric determination of acetylcholinesterase activity, Biochem. Pharmacol. 7 (1961) 88–95. doi:10.1016/0006-2952(61)90145-9.
[26] B. Ou, M. Hampsch-Woodill, R.L. Prior, Development and validation of an improved oxygen radical absorbance capacity assay using fluorescein as the fluorescent probe, J. Agric. Food Chem. 49 (2001) 4619–4626.
[27] A. Dávalos, C. Gómez-Cordovés, B. Bartolomé, Extending Applicability of the Oxygen Radical Absorbance Capacity (ORAC−Fluorescein) Assay, J. Agric. Food Chem. 52 (2004) 48–54. doi:10.1021/jf0305231.
[28] L. Fang, B. Kraus, J. Lehmann, J. Heilmann, Y. Zhang, M. Decker, Design and synthesis of tacrine-ferulic acid hybrids as multi-potent anti-Alzheimer drug candidates, Bioorg. Med. Chem. Lett. 18 (2008) 2905–2909. doi:10.1016/j.bmcl.2008.03.073.
[29] F. Denizot, R. Lang, Rapid colorimetric assay for cell growth and survival. Modifications to the tetrazolium dye procedure giving improved sensitivity and reliability, J. Immunol. Methods. 89 (1986) 271–277.
[30] C.M. Smith, C.K. Nolan, M.A. Edwards, J.B. Hatfield, T.W. Stewart, S.S. Ferguson, E.L. Lecluyse, J. Sahi, A comprehensive evaluation of metabolic activity and intrinsic clearance in suspensions and monolayer cultures of cryopreserved primary human hepatocytes, J. Pharm. Sci. 101 (2012) 3989–4002. doi:10.1002/jps.23262.
[31] M. Mennecozzi, B. Landesmann, T. Palosaari, G. Harris, M. Whelan, Sex Differences in Liver Toxicity—Do Female and Male Human Primary Hepatocytes React Differently to Toxicants In Vitro ?, PLOS ONE. 10 (2015) e0122786. doi:10.1371/journal.pone.0122786.
[32] L. Richert, A. Baze, C. Parmentier, H.H.J. Gerets, R. Sison-Young, M. Dorau, C. Lovatt, A. Czich, C. Goldring, B.K. Park, S. Juhila, A.J. Foster, D.P. Williams, Cytotoxicity evaluation using cryopreserved primary human hepatocytes in various culture formats, Toxicol. Lett. 258 (2016) 207–215. doi:10.1016/j.toxlet.2016.06.1127.
[33] L.F.N. Lemes, G. de Andrade Ramos, A.S. de Oliveira, F.M.R. da Silva, G. de Castro Couto, M. da Silva Boni, M.J.R. Guimarães, I.N.O. Souza, M. Bartolini, V. Andrisano, P.C. do Nascimento Nogueira, E.R. Silveira, G.D. Brand, O. Soukup, J. Korábečný, N.C. Romeiro, N.G. Castro, M.L. Bolognesi, L.A.S. Romeiro, Cardanol-derived AChE inhibitors: Towards the development of dual binding derivatives for Alzheimer's disease, Eur. J. Med. Chem. 108 (2016) 687–700. doi:10.1016/j.ejmech.2015.12.024.
[34] O. Trott, A.J. Olson, AutoDock Vina: improving the speed and accuracy of docking

with a new scoring function, efficient optimization, and multithreading, J. Comput. Chem. 31 (2010) 455–461. doi:10.1002/jcc.21334.
[35] E. Maalej, F. Chabchoub, M.J. Oset-Gasque, M. Esquivias-Pérez, M.P. González, L. Monjas, C. Pérez, C. de los Ríos, M.I. Rodríguez-Franco, I. Iriepa, I. Moraleda, M. Chioua, A. Romero, J. Marco-Contelles, A. Samadi, Synthesis, biological assessment, and molecular modeling of racemic 7-aryl-9,10,11,12-tetrahydro-7H-benzo[7,8]chromeno[2,3-b]quinolin-8-amines as potential drugs for the treatment of Alzheimer's disease, Eur. J. Med. Chem. 54 (2012) 750–763. doi:10.1016/j.ejmech.2012.06.038.
[36] Y. He, P.-F. Yao, S. Chen, Z. Huang, S.-L. Huang, J.-H. Tan, D. Li, L.-Q. Gu, Z.-S. Huang, Synthesis and evaluation of 7,8-dehydrorutaecarpine derivatives as potential multifunctional agents for the treatment of Alzheimer's disease, Eur. J. Med. Chem. 63 (2013) 299–312. doi:10.1016/j.ejmech.2013.02.014.
[37] M.-Y. Wu, G. Esteban, S. Brogi, M. Shionoya, L. Wang, G. Campiani, M. Unzeta, T. Inokuchi, S. Butini, J. Marco-Contelles, Donepezil-like multifunctional agents: Design, synthesis, molecular modeling and biological evaluation, Eur. J. Med. Chem. (n.d.). doi:10.1016/j.ejmech.2015.10.001.
[38] A. Cornish-Bowden, A simple graphical method for determining the inhibition constants of mixed, uncompetitive and non-competitive inhibitors (Short Communication), Biochem. J. 137 (1974) 143–144. doi:10.1042/bj1370143.
[39] R.B. Silverman, The Organic Chemistry of Enzyme-catalyzed Reactions, Academic Press, San Diego, 2000.
[40] M. Esquivias-Pérez, E. Maalej, A. Romero, F. Chabchoub, A. Samadi, J. Marco-Contelles, M.J. Oset-Gasque, Nontoxic and neuroprotective β-naphthotacrines for Alzheimer's disease, Chem. Res. Toxicol. 26 (2013) 986–992. doi:10.1021/tx400138s.
[41] K. Sugano, H. Hamada, M. Machida, H. Ushio, High Throughput Prediction of Oral Absorption: Improvement of the Composition of the Lipid Solution Used in Parallel Artificial Membrane Permeation Assay, J. Biomol. Screen. 6 (2001) 189–196. doi:10.1177/108705710100600309.
[42] F. Wohnsland, B. Faller, High-Throughput Permeability pH Profile and High-Throughput Alkane/Water log P with Artificial Membranes, J. Med. Chem. 44 (2001) 923–930. doi:10.1021/jm001020e.
[43] B.R. Brooks, R.E. Bruccoleri, B.D. Olafson, D.J. States, S. Swaminathan, M. Karplus, CHARMM: A program for macromolecular energy, minimization, and dynamics calculations, J. Comput. Chem. 4 (1983) 187–217. doi:10.1002/jcc.540040211.
[44] A. Morreale, F. Maseras, I. Iriepa, E. Gálvez, Ligand-receptor interaction at the neural nicotinic acetylcholine binding site: a theoretical model, J. Mol. Graph. Model. 21 (2002) 111–118. doi:10.1016/S1093-3263(02)00127-4.
[45] M. Bartolini, M. Pistolozzi, V. Andrisano, J. Egea, M.G. López, I. Iriepa, I. Moraleda, E. Gálvez, J. Marco-Contelles, A. Samadi, Chemical and Pharmacological Studies on Enantiomerically Pure p-Methoxytacripyrines, Promising Multi-Target-Directed Ligands for the Treatment of Alzheimer's Disease, ChemMedChem. 6 (2011) 1990–1997. doi:10.1002/cmdc.201100239.
[46] Gaussian 09, Revision C.01, Frisch, M. J.; Trucks, G. W.; Schlegel, H. B.; Scuseria, G. E.; Robb, M. A.; Cheeseman, J. R.; Scalmani, G.; Barone, V.; Mennucci, B.; Petersson, G. A.; Nakatsuji, H.; Caricato, M.; Li, X.; Hratchian, H. P.; Izmaylov, A. F.; Bloino, J.; Zheng, G.; Sonnenberg, J. L.; Hada, M.; Ehara, M.; Toyota, K.; Fukuda, R.; Hasegawa, J.; Ishida, M.; Nakajima, T.; Honda, Y.; Kitao, O.; Nakai, H.; Vreven, T.; Montgomery Jr., J. A.; Peralta, J. E.; Ogliaro, F.; Bearpark, M. J.; Heyd, J.; Brothers, E. N.; Kudin, K. N.; Staroverov, V. N.; Kobayashi, R.; Normand, J.; Raghavachari, K.; Rendell, A. P.; Burant, J. C.; Iyengar, S. S.;

Tomasi, J.; Cossi, M.; Rega, N.; Millam, N. J.; Klene, M.; Knox, J. E.; Cross, J. B.; Bakken, V.; Adamo, C.; Jaramillo, J.; Gomperts, R.; Stratmann, R. E.; Yazyev, O.; Austin, A. J.; Cammi, R.; Pomelli, C.; Ochterski, J. W.; Martin, R. L.; Morokuma, K.; Zakrzewski, V. G.; Voth, G. A.; Salvador, P.; Dannenberg, J. J.; Dapprich, S.; Daniels, A. D.; Farkas, Ö.; Foresman, J. B.; Ortiz, J. V.; Cioslowski, J.; Fox, D. J.; Gaussian, Inc.: Wallingford, CT, USA, 2009.

[47] K. Raghavachari, Perspective on "Density functional thermochemistry. III. The role of exact exchange," in: P.C.J. Cramer, P.D.G. Truhlar (Eds.), Theor. Chem. Acc., Springer Berlin Heidelberg, 2000: pp. 361–363. doi:10.1007/978-3-662-10421-7_60.

[48] null Lee, null Yang, null Parr, Development of the Colle-Salvetti correlation-energy formula into a functional of the electron density, Phys. Rev. B Condens. Matter. 37 (1988) 785–789.

List of captions

Figures

Figure 1. Structures of tacrine, clioquinol, and the new racemic 7-aryl-9,10,11,12-tetrahydro-7*H*-pyrano[2,3-b:5,6-h']diquinolin-8-amine derivatives (**I**) described in this work.

Figure 2. Lineweaver – Burk plot illustrating non-competitive type of hAChE inhibition by compound **2h**. S = acetylthiocholine; *V* = initial velocity rate.

Figure 3. B3LYP-optimized structures for Cu^{2+} complexes of PPQ.

Figure 4. B3LYP-optimized structures for Cu^{2+} complexes of PhePQ.

Figure 5. Binding mode of (*R*)-**2h** at the active site of hAChE: Binding affinity = -11.3 Kcal mol^{-1}. The compound is rendered as balls and sticks and illustrated in blue. The side chains conformations of the mobile residues are illustrated in the same light color that the ligand. Different sub-sites of the active site were coloured: catalytic triad (CT) in green, oxyanion hole (OH) in pink, anionic sub-site (AS) in orange, except Trp86, acyl binding pocket (ABP) in yellow, except Phe297 and Phe338, and peripheral anionic sub-site (PAS) in violet**.** Red dashed lines are drawn among atoms involved in hydrogen bond interactions.

Figure 6. a) Schematic representation of different interactions of (*R*)-**2h** with hAChE.
b) Top view of the accessible surface of the active site gorge**.**

Figure 7. Binding mode of (*S*)-**2h** at the active site of hAChE: Binding affinity = -10.8 Kcal mol^{-1}; The compound is rendered as balls and sticks and illustrated in pink. The side chains conformations of the mobile residues are illustrated in the same light color that the ligand. Different sub-sites of the active site were coloured: catalytic triad (CT) in green, oxyanion hole (OH) in pink, anionic sub-site (AS) in orange, except Trp86, acyl binding pocket (ABP) in yellow, except Phe297 and Phe338, and peripheral anionic sub-site (PAS) in violet**.** Red dashed lines are drawn among atoms involved in hydrogen bond interactions.

Figure 8. a) Schematic representation of different interactions of (*S*)-**2h** with hAChE.
b) Top view of the accessible surface of the active site gorge.

Figure 9. Overlay of binding mode of compound (*R*)-**2h** (blue) and (*S*)-**2h** (pink) in hAChE.

Schemes

Scheme 1. Synthesis of racemic tetrahydropyranodiquinolin-8-amines **2a-l**.

Scheme 2. Chemical equations used to measure the formation energies of the complexes $[Cu(II)(PPQ)(MeOH)_x(SO_4)]$.

Scheme 3. Chemical equations used to measure the formation energies of the complexes $[Cu(PhePQ)(MeOH)_x(SO_4)]$.

Tables

Table 1. Inhibition of *Ee*AChE, hACHE, eqBuChE, (IC_{50}, □M) and ORAC-FL values for compounds **2a-l** , tacrine, clioquinol and ferulic acid.

Table 2. Thermodynamic functions of the copper (II) complexes with PPQ.

Table 3. Thermodynamics functions of the copper (II) complexes with PhePQ.

Table 4. Selected theoretical geometrical parameters for Cu(PPQ)(SO_4) and Cu(PhePQ)(SO_4) complexes[a].

Table 5. Selected atomic charges for Cu(PPQ)(SO_4) and Cu(PhePQ)(SO_4)

Table 6. *In vitro* cytotoxicity of tacrine, **2a**, **2c** and **2h-j** in HepG2 cells.

Table 7. *In vitro* concentration-response of tacrine and **2h** on primary human *hepatocyte viability*

Table 1. Inhibition of *Ee*AChE, hACHE, eqBuChE, (IC_{50}, μM) and ORAC-FL values for compounds **2a-l** , tacrine, clioquinol and ferulic acid.

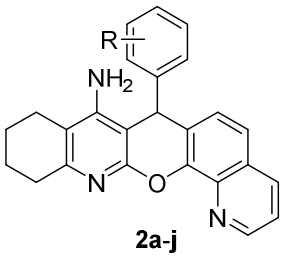

2a-j

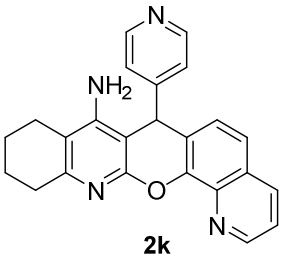

2k

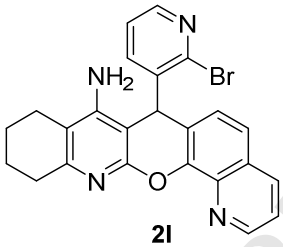

2l

Compound	R	*Ee*AChE[a]	hAChE	eqBuChE[a]	BBB	ORAC
2a	H	0.06±0.01	1.73 ± 0.02	1.11±0.00	-[c]	1.47±0.25
2b	2-F	0.11±0.01	-[c]	0.63±0.08	-[c]	1.49±0.09
2c	3-F	0.09±0.01	2.20 ± 0.03	-[d]	-[c]	1.36±0.05
2d	2-Br	0.14±0.01	-[c]	0.21±0.02	-[c]	2.01±0.05
2e	4-NO_2	0.24±0.01	-[c]	-[d]	-[c]	2.49±0.19
2f	2,6-di-Cl	0.10±0.01	-[c]	-[d]	-[c]	1.22±0.07
2g	2-OCH_3	0.08±0.01		1.51±0.10	-	1.60±0.22
2h	**3-OCH_3**	**0.04±0.01**	**0.75 ± 0.01**	**1.30±0.22**	**5.41 ± 0,3[b]**	**1.83±0.10**
2i	4-OCH_3	0.04±0.01	1.51 ± 0.02	1.30±0.19	-[c]	1.71±0.10
2j	4-CH_3	0.04±0.01	2.85 ± 0.05	0.53±0.03	-[c]	1.88±0.35
2k	-	0.47±0.07	-[d]	-[d]	-[c]	1.70±0.12
2l	-	0.19±0.00	-[d]	2.86±0.18	-[c]	2.35±0.26
Tacrine	-	0.03±0.01	0.13±0.00	0.05±0.01nM	-[c]	0.2±0.1
Ferulic acid	-	-[c]	-[c]	-[c]	-[c]	3.74±0.22

[a] Inhibition curves were obtained by nonlinear regression. *Ee*: electric eel, eq: equine. Each IC_{50} value is the mean ± SEM of quadruplicate of at least three different experiments. Results are expressed in μM; [b] PAMPA method (Pe ± SEM (*10^{-6} cm s^{-1}); [c]Not determined ; [d] No inhibition.

Table 2. Thermodynamic functions of the copper (II) complexes with PPQ.

Complex	ΔH(Kcal/mol)	ΔG(Kcal/mol)
Cu(PPQ)(SO_4)	0.61	-7.85
Cu(PPQ)(SO_4)(MeOH)	5.69	-2.77

Table 3. Thermodynamics functions of the copper (II) complexes with PhePQ.

Complex	ΔH(Kcal/mol)	ΔG(Kcal/mol)
Cu(PhePQ)(SO_4)	-2.02	-9.99
Cu(PhePQ)(SO_4)(MeOH)	3.52	-4.22

Table 4. Selected theoretical geometrical parameters for Cu(PPQ)(SO_4) and Cu(PhePQ)(SO_4) complexes[a].

Complex	d_{C-O}	d_{Cu-O}	d_{Cu-N}
Cu(PPQ)(SO_4)	1.397	2.321	1.994
Cu(PhePQ)(SO_4)	1.410	2.260	1.971

[a] d, bond distance in Å.

Table 5. Selected atomic charges for $Cu(PPQ)(SO_4)$ and $Cu(PhePQ)(SO_4)$ complexes.

Complex	O charge
$Cu(PPQ)(SO_4)$	-0.476
$Cu(PhePQ)(SO_4)$	-0.517

Table 6. *In vitro* cytotoxicity of tacrine, **2a**, **2c** and **2h-j** in HepG2 cells.

	30 µM	**100 µM**	**300 µM**	**1000 µM**
Tacrine	106.4 ± 6.1	110.5 ± 5.8	49.3 ± 3.7***	13.7 ± 3.1***
2a	108.6 ± 12.8	102.2 ± 11.2	93.7 ± 11.5	91.2 ± 6.4
2c	92.4 ± 3.4	95.4 ± 11.5	91.6 ± 13.9	75.8 ± 5.7*
2h	110.0 ± 3.5	102.2 ± 5.2	94.0 ± 7.4	94.1 ± 3.0
2i	115.4 ± 1.7	110.7 ± 3.8	113.8 ± 4.0	104.7 ± 1.4
2j	115.9 ± 4.9	106.0 ± 1.5	92.5 ± 5.9	96.2 ± 4.8

Means ± SEM of triplicates from at least three different cultures. *$p<0.05$, ***$p<0.001$, as compared to the control cultures (one-way ANOVA).

Table 7. *In vitro* concentration-response of tacrine and **2h** on primary human *hepatocyte viability*

Concentration	00 μM	0.1 μM	1.0 μM	3.0 μM	10.0 μM	30.0 μM	100.0 μM
Tacrine	100 ± 11	94 ± 3	86 ± 3	83 ± 5	81 ± 7	75 ± 14	70 ± 3
2h	100 ± 11	89 ± 4	84 ± 8	83 ± 8	89 ± 3	99 ± 11	89 ± 2

Results expressed in Means ± SD of triplicates from from a pool of 9 donors

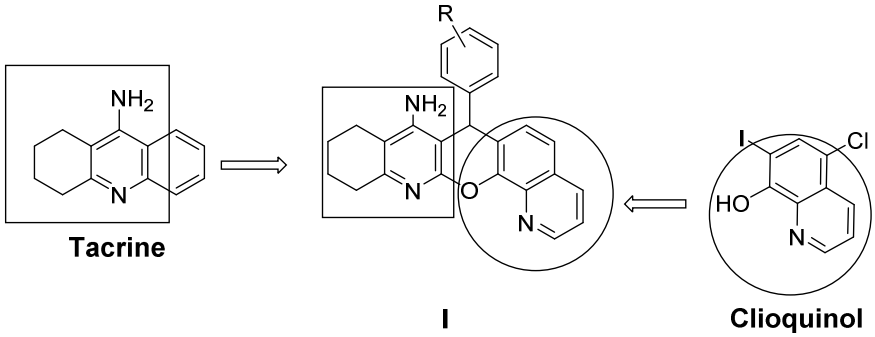

Figure 1 Structures of tacrine, clioquinol, and the new racemic 7-aryl-9,10,11,12-tetrahydro-7*H*-pyrano[2,3-b:5,6-h']diquinolin-8-amine derivatives (**I**) described in this work.

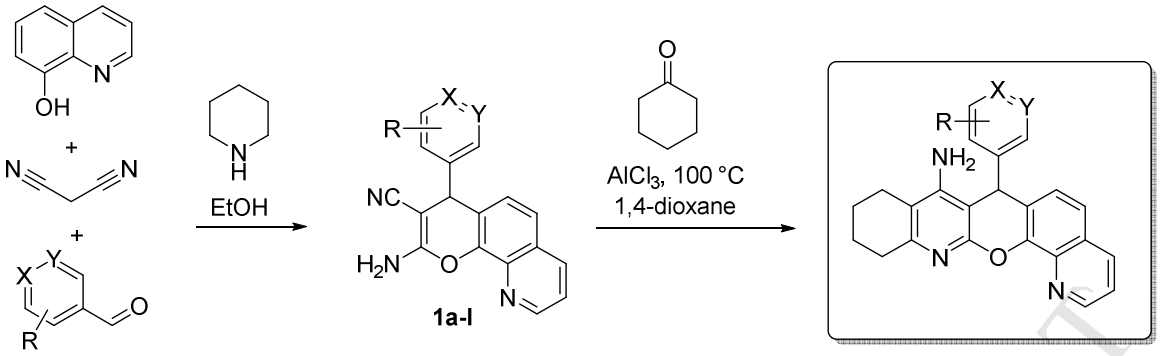

Scheme 1. Synthesis of racemic tetrahydropyranodiquinolin-8-amines **2a**-**l**.

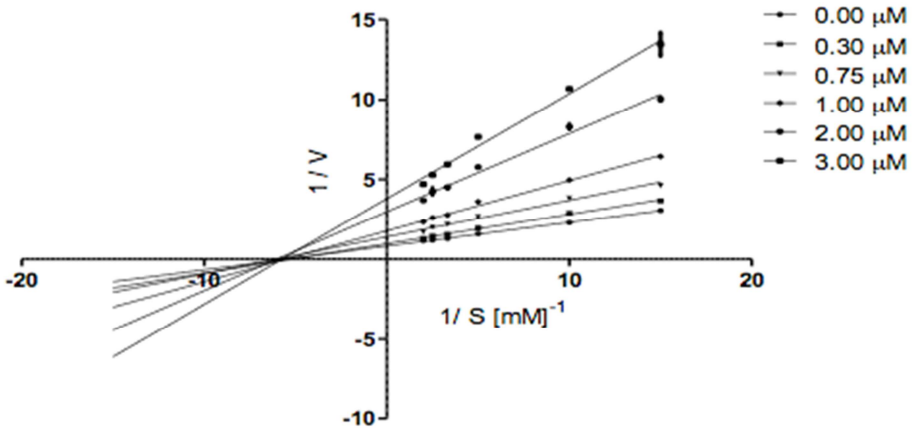

Figure 2. Lineweaver – Burk plot illustrating non-competitive type of hAChE inhibition by compound **2h**. S = acetylthiocholine; *V* = initial velocity rate.

[E (Cu(PPQ)(SO_4) + 2 E(MeOH)] – [E(PPQ) + E (Cu (II) $(MeOH)_2(SO_4)$] (I)

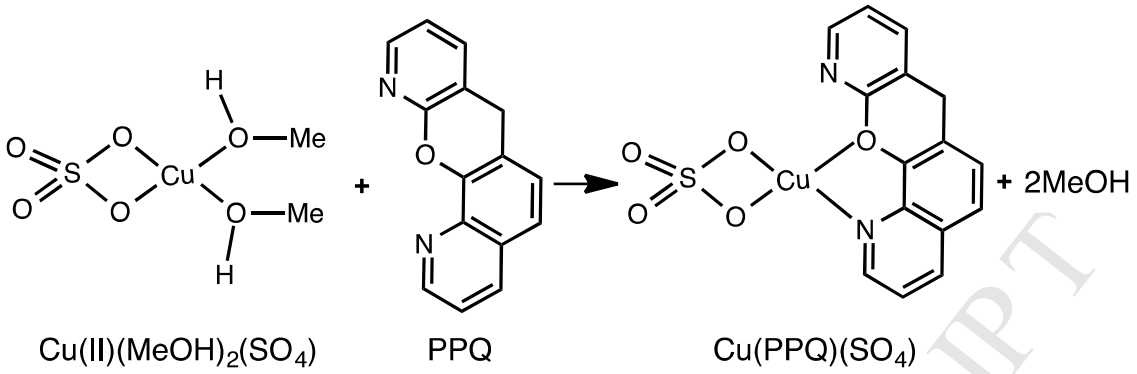

[E (Cu(PPQ)(SO_4)(MeOH)) + 2 E(MeOH)] – [E(PPQ) + E (Cu (II) $(MeOH)_3(SO_4)$] (II)

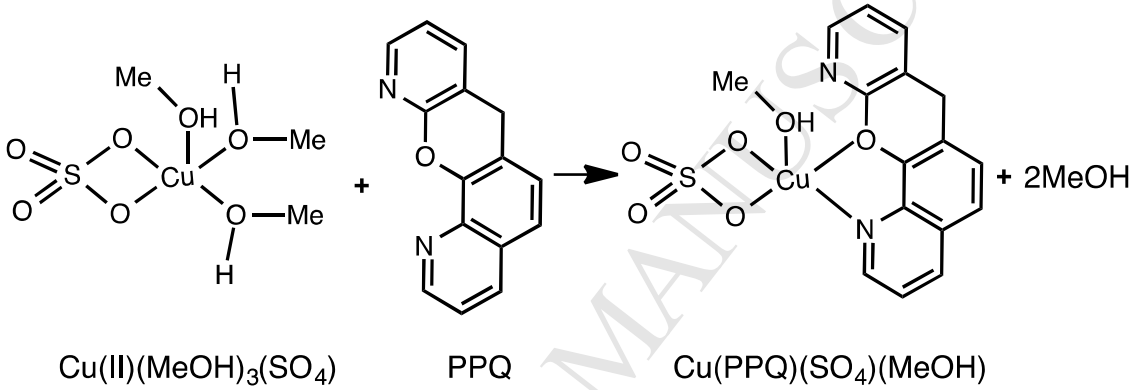

Scheme 2. Chemical equations used to measure the formation energies of the complexes [Cu(II)(PPQ)$(MeOH)_x(SO_4)$].

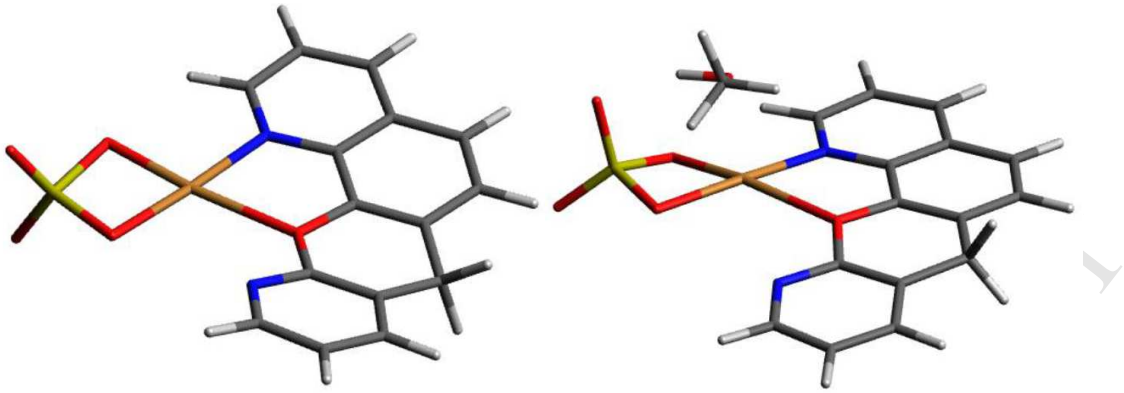

Cu(PPQ)SO_4 Cu(PPQ)SO_4(MeOH)

Figure 3. B3LYP-optimized structures for Cu^{2+} complexes of PPQ.

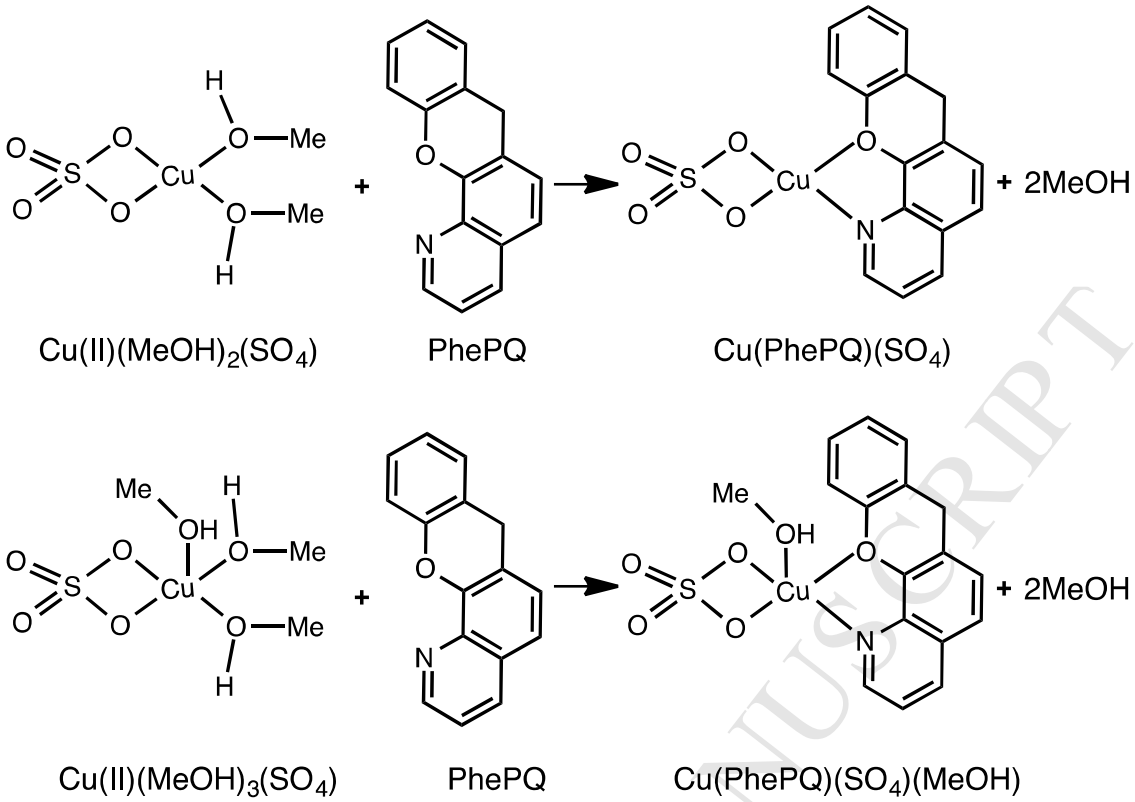

Scheme 3. Chemical equations used to measure the formation energies of the complexes [Cu(PhePQ)$(MeOH)_x(SO_4)$].

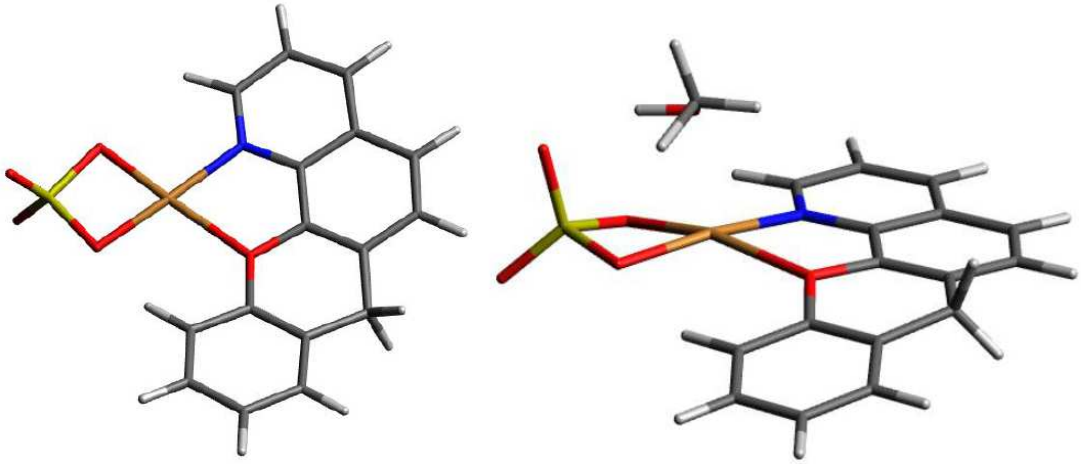

Cu(PhePQ)(SO_4) Cu(PhePQ)(SO_4)(MeOH)

Figure 4. B3LYP-optimized structures for Cu^{2+} complexes of PhePQ.

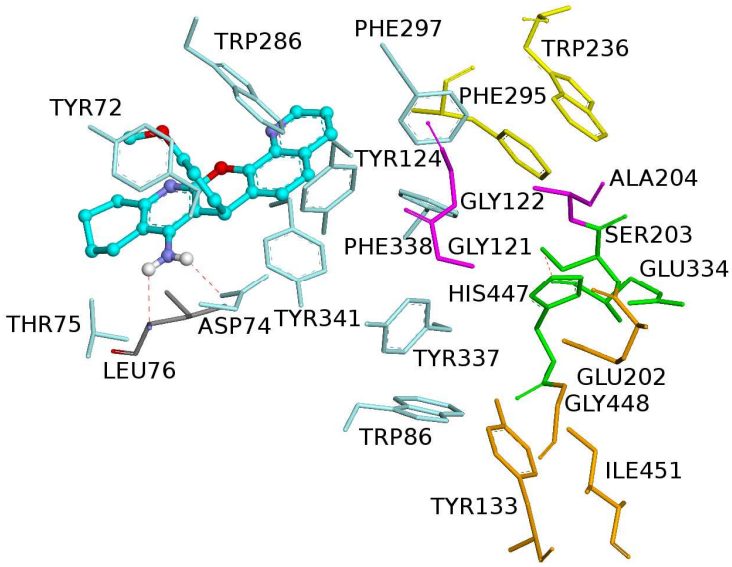

Figure 5. Binding mode of (*R*)-**2h** at the active site of hAChE: Binding affinity = -11.3 Kcal mol^{-1}. The compound is rendered as balls and sticks and illustrated in blue. The side chains conformations of the mobile residues are illustrated in the same light color that the ligand. Different sub-sites of the active site were coloured: catalytic triad (CT) in green, oxyanion hole (OH) in pink, anionic sub-site (AS) in orange, except Trp86, acyl binding pocket (ABP) in yellow, except Phe297 and Phe338, and peripheral anionic sub-site (PAS) in violet**.** Red dashed lines are drawn among atoms involved in hydrogen bond interactions.

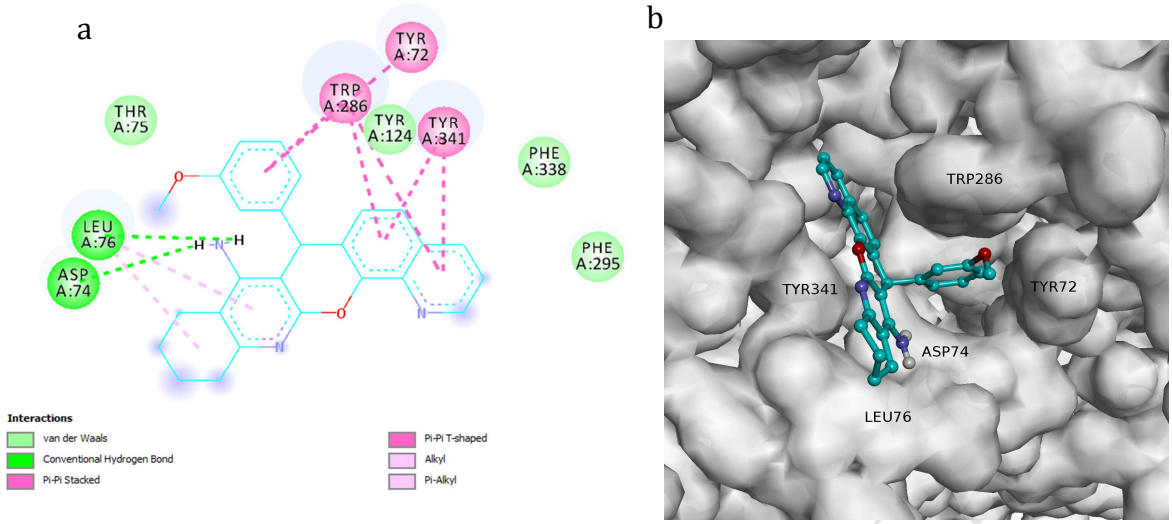

Figure 6. a) Schematic representation of different interactions of (*R*)-**2h** with hAChE. b) Top view of the accessible surface of the active site gorge**.**

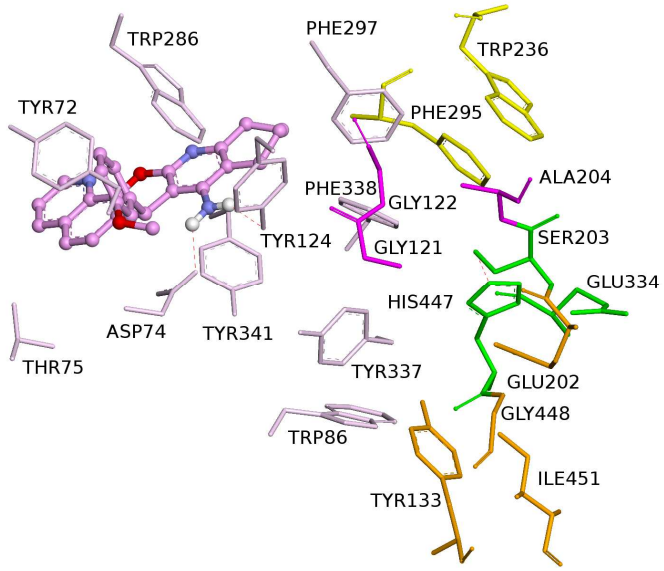

Figure 7. Binding mode of (*S*)-**2h** at the active site of hAChE: Binding affinity = -10.8 Kcal mol^{-1}; The compound is rendered as balls and sticks and illustrated in pink. The side chains conformations of the mobile residues are illustrated in the same light color that the ligand. Different sub-sites of the active site were coloured: catalytic triad (CT) in green, oxyanion hole (OH) in pink, anionic sub-site (AS) in orange, except Trp86, acyl binding pocket (ABP) in yellow, except Phe297 and Phe338, and peripheral anionic sub-site (PAS) in violet**.** Red dashed lines are drawn among atoms involved in hydrogen bond interactions.

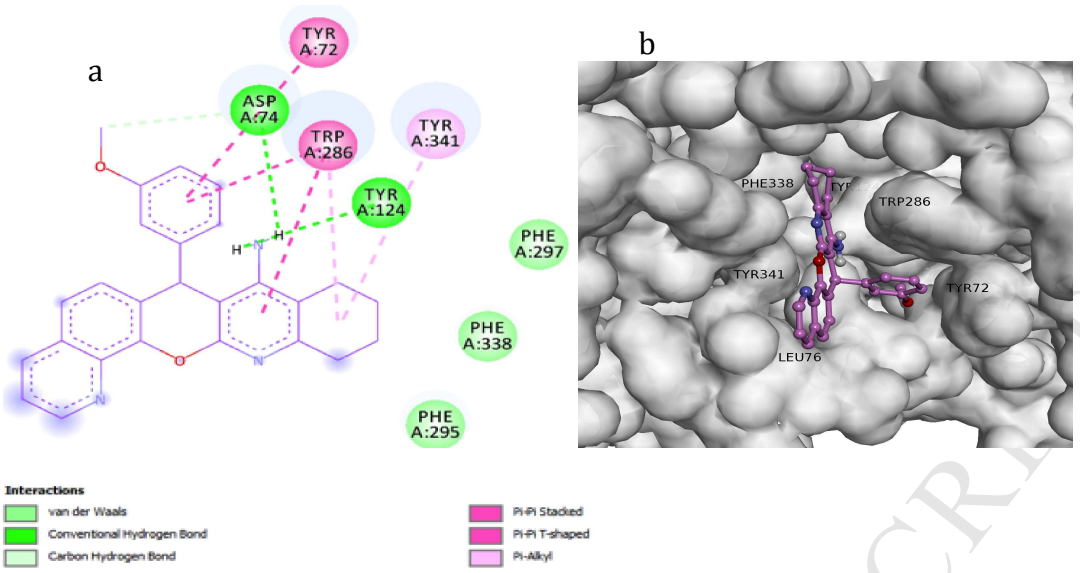

Figure 8. a) Schematic representation of different interactions of (*S*)-**2h** with hAChE. b) Top view of the accessible surface of the active site gorge.

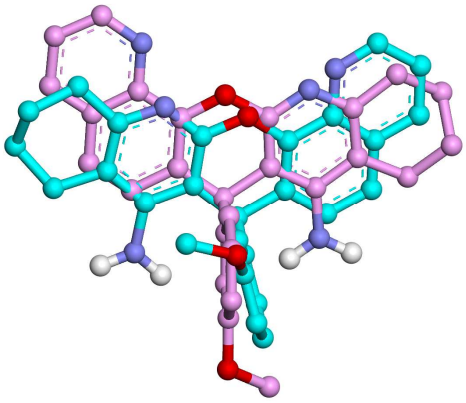

Figure 9. Overlay of binding mode of compound (*R*)-**2h** (blue) and (*S*)-**2h** (pink) in hAChE.

Highlights

12 novel multitarget directed ligands for Alzheimer's disease

The *in vitro* enzymatic and hepatotoxic activities were evaluated

The primary structure–activity relationships were discussed

Compound **2h** is non-hepatotoxic, and selective hAChE inhibitor